Use Authorization

In presenting this thesis in partial fulfillment of the requirements for an advanced degree at Idaho State University, I agree that the Library shall make it freely available for inspection. I further state that permission to download and/or print my thesis for scholarly purposes may be granted by the Dean of the Graduate School, Dean of my academic division, or by the University Librarian. It is understood that any copying or publication of this thesis for financial gain shall not be allowed without my written permission.

Signature _____

Date _____

PARAMETRIC ANALYSIS OF THE BEHAVIOR OF ULTRA HIGH PERFORMANCE CONRETE UNDER HIGH FREQUENCY DIRECT SHEAR LOADING

by

Colton Bedke

A thesis

submitted in partial fulfillment

of the requirements for the degree of

Master of Science in the Department of Civil and Environmental Engineering Idaho State University

Spring 2016

Committee Approval

To the Graduate Faculty:

The members of the committee appointed to examine the thesis of COLTON BEDKE find it satisfactory and recommend that it be accepted.

_____

Major Advisor

Dr. Andrew Sorensen

_____

Committee Member

Dr. Arya Ebrahimpour

_____

Graduate Faculty Representative

Dr. Marco Schoen

Table of Contents

List of Tables

List of Figures

PARAMETRIC ANALYSIS OF THE BEHAVIOR OF ULTRA HIGH PERFORMANCE CONRETE UNDER HIGH FREQUENCY DIRECT SHEAR LOADING

Thesis Abstract

Idaho State University (2016)

This study investigates the behavior associated with Ultra High Performance Concrete (UHPC) subjected to a high frequency direct shear loading. UHPC is a concrete that eliminates the use of a course aggregate, utilizes a low water to cement ratio, develops a pozzolonic reaction through the use of silica fume, and has a compressive strength exceeding 21 ksi. High frequency direct shear loading is typically observed when an object is exposed to a blast loading; either by direct impact or the blast energy as the result of an explosion. The use of UHPC is relatively new throughout the world and therefore the mechanical properties are lesser known compared to other structural materials. Once a UHPC mix design is established through the use of local materials, components of the design mix are altered to determine their effect on the shear strength and energy absorption. The parameters observed in this study are: percentage of silica fume, water to binder ratio, and fine sand gradation. The compressive strength is determined through standard ASTM methods and the energy absorption is determined using Charpy Impact testing methods. This presentation aims to present the results obtained through the laboratory testing. From these results, trends are observed on the impact of each parameter to the energy absorption. Ultimately an optimum UHPC mix can be selected.

CHAPTER 1

INTRODUCTION

1.1 Background and Motivation

Research into blast and impact loads' effects on buildings and other structures has been an ever-growing topic. As terrorist activity has continued to grow and adapt, this type of loading conditions have become more frequent. As blast loads become more recurrent, it is no longer impractical to design a building that takes into account blast loads. Previous research has primarily focused on the macro-behavior of a structure under such loads (Ma et. al, 2010; Naito et. al, 2006; Huang et. al, 2011; Krauthammer et. al, 1986). However, minimal research has been conducted on the investigation of the micro-structure of the materials under these blast and impact loads.

As material sciences continue to advance and improve our structural resources, the behavior of these materials is also continually studied. New developments of structural concrete has yielded a classification of concrete known as Ultra-High Performance Concrete (UHPC). This concrete has a superior compressive strength compared to that of typical normal weight concrete. UHPC is defined as "A cementitious composite material composed of an optimized gradation of granular constituents, a water-to-cementitious materials ratio less than 0.25, and a high percentage of discontinuous internal fiber reinforcement. The mechanical properties of UHPC include compressive strengths greater than 21.7 ksi…"(Graybeal, 2011). Through the literature review, multiple authors have defined varying compressive strengths that qualify for UHPC. For this study, a compressive strength exceeding 20 ksi classifies the mix as a UHPC.

The compressive strength of UHPC far exceeds that of normal weight concrete which typically falls in the range of 6-8 ksi. It is found through further research that other mechanical properties of UHPC are also superior to that of normal weight concrete. Some of these properties include but are not limited to: split tensile strength, flexural strength, modulus of elasticity, shrink-swell behavior, water absorption, chloride ion penetration, freeze-thaw durability, scaling resistance, and abrasion resistance (Allena et. al, 2001; Prem et. al, 2012; Graybeal and Tanesi, 2007; Magureanu et. al, 2012; Wille et. al, 2011).

In the analysis of structures exposed to blast and impact loading, through the development of Pressure-Impulse (PI) diagrams, a damage assessment can be conducted on a component of a structure such as a wall. Through these PI diagrams, as the pressure decreases the impulse increases. When the impulse of a blast reaches maximum levels, a given wall is more likely to fail in shear as opposed to flexural bending. (Natio et. al, 2006; Huang et. al2011). The mechanical properties on a micro-level of UHPC are well known when it comes to flexural and cracking strengths. However the shear strength of UHPC is a lesser investigated behavior. Not knowing these mechanical behaviors makes it difficult to design for a structure that could possibly undergo a blast load that exhibits a high impulse. The nature of PI diagrams and also the mechanical behaviors of UHPC are further discussed in Chapter 2.

1.2 Problem Definition and Scope

As stated in the previous section, the contemporary research has focused on blast loads on structures and how they can be properly modeled. These models accurately depict damage assessments for a given blast load and radius. However the research neglects to examine the failure modes at a micro-level of the material. This current

research intends to examine what is occurring in the UPHC micro-structure under high frequency impact loading.

The relatively new and current research into UHPC has provided for knowledge into the mechanical behaviors of the material. However, with all this research, the shear strength of UHPC under high frequency impact loading has been overlooked. This current study will use a parametric approach in analyzing the shears strengths of UHPC under impact loading through energy absorption rates.

This thesis proposes the following questions to determine the impact energy absorption and ultimately the shear strength of UHPC under impact loading:

1. Can an impact load be modeled on UHPC specimens that allows the micro-level behavior to be examined? From this model, can the resulting impact energy be obtained?
2. Can a mix design from local materials that meets the requirements as a UHPC be established? From this mix design, can a parametric study be conducted to examine the associated mechanical properties?

In addressing these questions, this thesis will expand on not only the knowledge of structures under impact loading at the micro-level, but also further develop the information of UHPC and its mechanical properties associated with shear strengths and energy absorption.

1.3 Objectives

In order to answer the previously stated questions, the objectives of this thesis are to:

1. Develop accurate testing methods to determine the compressive strength for UHPC specimens.
2. Establish mixing and curing methods that result in a control mix design using local materials. This mix design must meet the criteria of a UHPC.
3. Determine the available mix design parameters of UHPC to study their effect on the energy absorption.
4. Develop a testing method that accurately models a high frequency impact load on a given specimen.
5. Observe any correlation between the compressive strength and energy absorption of UHPC.
6. Determine an optimum mix design to increase energy absorption of UHPC mixes.

1.4 Research Tasks and Methodology

Laboratory studies are essential and will be the primary method to complete the objectives stated in the previous section. Although UHPC is available commercially, a parametric study is not feasible using a pre-mixed, proprietary product. Therefore, designing a mix using locally available constituents is the first task to complete this research. In order to verify the acceptability of the mix, proper compressive strength testing is required. Due to UPHC's extremely high strengths, traditional testing methods typically aren't feasible in the testing. Once a UHPC is produced and verified by proper testing methods, the parametric study can be initiated.

In order to conduct the parametric study, different components of the mix design are altered. The components to be altered are water to binder ratio (w/b ratio), percent silica fume replacement, and fine sand gradation. The w/b ratio is increased and decreased by 2.5% and 5% from the control mix. The silica fume is increased and decreased by 5% and 10% from the control mix. The sand gradation varies the size of the sand particles and the proportions for each size.

Once the mix designs are calculated, each design is mixed and cast. From these designs, both compressive and Charpy impact samples are cast from the same batch. The casting procedures follow all ASTM standards, where applicable. After they are cast, the samples are allowed to cure in their molds for 24 hours. They are then removed from their molds and placed into a heated curing regime for the remaining 28 days. This curing regime utilizes both a lime water bath method as well as oven curing to maintain higher temperatures during the curing process. This allows for a pozzolonic reaction to occur within the cement matrix and the silica fume.

At the end of the 28 days of curing the samples are removed and tested. Each sample's dimensions are measured appropriately and then tested to its respective method. At the conclusion of the testing, the data is collected and analyzed. Results and conclusions are then made for each parameter of the study. A complete detail for the methodology for this thesis is provided in Chapter 3.

1.5 Thesis Overview

The entirety of this thesis contains five chapters. The current chapter (Chapter 1) provides for a brief overview of the thesis. Chapter 2 provides a detailed literature review of relevant research associated with this thesis. It is broken into three sections; the first

focuses on research associated with blast loading, the second on research associated with Charpy impact testing, and the third on research associated with UHPC mix designs and its mechanical properties. Chapter 3 provides the methodology that is followed to meet the objectives of this thesis. This includes the steps taken in the mix design, casting, and testing of the specimens. Testing materials and setup is also included. Chapter 4 provides the results that are obtained in the laboratory testing of the UHPC specimens and trends that are observed. Lastly Chapter 5 outlines the conclusions made in this thesis. The thesis also includes appendices that include the mix proportions, individual measurements, and results for each UHPC specimen as well as specific details and composition of each material used.

CHAPTER 2

LITERATURE REVIEW

2.0 Introduction

This chapter presents a literature review on previous research conducted relevant to the research carried out in this thesis. This chapter is divided into four main sections. The first section focuses on blast and impact loads and how to model these loads on concrete structures. The second section of this chapter looks at the Charpy impact testing method. The third section deals with the mix designs of Ultra High Performance Concrete (UHPC) and its associated mechanical properties. The final section summarizes the findings and how they apply to the current study.

2.1 Blast Load Models

2.1.1 Simplified Blast Load Assessments

The study carried out by Ma and others (2010) investigates the effects of blast loads on buried structures and the soil-structure interactions (SSI). Previous studies have conducted similar research using single degree of freedom (SDOF) models. However, this method is invalid when considering structures that undergo a mixed failure mode of both shear and flexural failure. This study by Ma and others (2010) extends the use of previous studies of the use of pressure-impulse (P-I) diagrams to also include the effects of the SSI as well as mixed failure modes. Special conditions are examined to verify the continuity between results for the different failure modes.

When determining the effects of the SSI, a one unit strip of wall is analyzed as a simply supported beam. The beam is loaded with a simulated blast load modeled by a

uniform load across the entire span. Constants are obtained through experimental study to account for the SSI. Through the derivation of equations, blast loads can be calculated as well as a shear-to-bending ratio. This ratio can be used to determine what type of failure mode the beam experiences, whether it be purely in shear, bending, or a combination of both. Using this ratio a displacement due to bending and shear can be calculated and a P-I diagram can be obtained to determine the damage a structure has undergone.

The analysis by Ma and others (2010) successfully accounts for the SSI effects for blast loads on structures. P-I diagrams are successfully developed to account for those effects that had not been accounted for in previous studies. It is concluded through these analyses that maximum shear displacement is more sensitive than the bending displacement resulting from the pressure applied. The present study uses this research to aid in determining the shear strength of concrete while under a blast load. The study by Ma and others (2010) also verifies the continuity between failure modes. Continuity is determined between bending failure and the different modes of mixed failure. However it fails to verify any continuity between failure purely by shear and any other of the failure modes.

2.1.2 Concrete Shear Wall Blast Assesment

In past studies, analyzing a structure subjected to a blast load could be difficult and take significant amount of time to compute. In a 2006 study by Naito and others, the researchers look at simplifying this process (Naito et. Al., 2006). In using a SDOF, basic section analyses and static finite element pushover analysis; a more effective method may be used in making blast assessments to structures. By utilizing a SDOF, one can cut down on computational time in accounting for material non-linearities and dynamic actions.

Critical displacements that signify failure stages are determined by the use of plastic hinges as well as the non-linear material behavior. With that information gained, P-I diagrams can be produced in order to quantify how well a structure will resist a blast load.

Before a structure is analyzed for a blast load, a static pushover analysis is conducted on the wall system. This approximates where a failure will1 occur in the wall from a given blast. This location is determined to be the corner of a structure. A pressure distribution from a given blast is then assumed as well as the location of the explosion. The structure, floor diaphragm, walls, and coupling beams are all assumed to be rigid with respect to blast pressure as well. Finite element models are then used in determining the stresses experienced by the wall components.

From these models one can determine when and where the plastic hinges will form; they form once an element has reached it yielding moment. Through the formation of plastic hinges the critical displacements are known and are used as benchmarks that portrays the inelastic behavior and its different stages. The blast load that is applied to the structure is approximated as a triangular distribution. The impulse is then calculated as the area under the curve of the max positive pressure applied over a time duration.

The equivalent SDOF requires the input of the max pressure as well as the impulse. A stepwise approach is used by calculating both of these at intervals until either the ultimate displacement is reached or until the demand is too low and the system rebounds. Using this information P-I curves can be developed to assess the damage of a structure that has experienced a blast load. If one hinge has formed the structure is considered to be at the immediate occupancy level. The integrity of this structure has not

been compromised and is still safe to occupy. A structure that has formed two plastic hinges it is classified as life safety level. At this level the wall has been damaged but the overall integrity of the system remains at safe levels for occupancy. However if they system develops a third plastic hinge it is classified as the collapse level. At this point the structure must have some sort of protection or the system will collapse.

The present study looks at the shear strengths of UHPC. A specimen that is under a short duration shear load exhibits the same characteristics as one under a blast load. The study by Naito and others (2006) looks at how to model systems under a blast load. This present study attempts to follow the model set forth by Naito and others, however it will look as single elements as opposed to an entire system.

One issue with the model set forth by Naito and others (2006) is the fact that they only look at how a system reacts due to the bending moments on a structure's components. The authors point out that shear failure is not considered in their study. It is very possible for a system to fail if the impulse is high enough to reach the yield stresses for shear before the elements have had a chance to respond in flexure. Although the present study doesn't look at a system as a whole, it does look at how single elements of UHPC will be affected by direct shear loading.

2.1.3 Soil Structure Interaction Diagrams

In a study conducted by Huang and others (2011), P-I diagrams are developed using the classical mode approximation method (MAM). These diagrams are used to assess the damage of a structure that is subjected to a blast load. Although MAM can be very effective to generate these P-I diagrams based purely on the beam element and its properties, there are other outside factors that affect the results. This study looks at both

internal and external blast loads and how to derive the P-I equations, and how a non-constant SSI affects the damage assessment.

In this study a simply supported beam is used to model a strip wall from an underground protective structure. The P-I equations that are derived are based on different modes which take into account the deformed shape of the beam and what stresses cause the deformation. The SSI is simplified to a non-constant damping coefficient to take into account any deformation in the soil due to the blast load. These P-I equations also take into account three different pulse shapes: triangular, rectangular, and exponential. Once a diagram is developed, it is used to assess the structure. If the structure is located to the left or bottom of the curve, then the displacement is small enough for the structure to be considered safe.

Huang and others (2011) found that the pulse shape for underground structures cannot be ignored when developing the P-I equations. The rectangular and triangular pulse shape both overestimate the structural response. It is also determined that when the blast duration is short, the non-constancy of SSI causes the P-I diagram to be much more sensitive in both external and internal blasts. It is recommended in the design of underground reinforced concrete to use the exponential pulse shape as well as a non-constant SSI. This study looks at simplifying the SSI to a non-constant damping coefficient. The damping coefficient is inversely related to the blast load duration. The equation is then assumed to find the damping coefficient. Although this theoretical equation has merit, there has been no experimental studies carried out to confirm the accuracy of the damping coefficient. Further study of this damping coefficient could possibly lead to more accurate results for the P-I diagrams in this study.

2.1.4 Modified Single Degree of Freedom

In order to analyze shallow-buried reinforced concrete (RC) box-type structure under a blast and shock loads, Krauthammer and others (1986) have an improved SDOF model. This model incorporates the effects of flexure, shear, thrust, and the SSI during the analysis of extreme dynamic loading. In order to develop this improved SDOF approximation, both field and lab tests are combined with theoretical and empirical equations to model the behavior of the RC box-type structures under the blast and shock loads.

In this study, the test specimens are scaled down and buried under a shallow backfill of soil. The specimens are then loaded by a pressure pulse applied through the soil surface. Results are obtained by recording the strains, accelerations, peak relative displacements, soil stresses, interface pressures, blast pressures and examination of specimens before and after testing. In order to assess the performance of the shallow-buried RC specimens, different behaviors and parameters such as: externally applied thrust, dynamic shear resistance, damping ratio, and effective mass are all determined through methods defined in previous studies. These are combined with a computational flow diagram developed by Krauthammer and others (1986) in the assessment of the structures.

Through this process developed by Krauthammer and others (1986), they are able to obtain theoretical results within 10% of the experimental data. They are also able to accurately specify the time at which the test specimens failed in shear. However it is determined that the methods used are very sensitive to the mechanical systems. This

sensitivity can cause errors in the results if careful considerations are not taken to prevent this.

2.1.5 Concrete Damage Under Impact

In the study conducted by Koh and others (2001), the damage effects of impact loads on concrete is observed both numerically and experimentally. Due to concrete's complex properties, a model must be developed that accounts for the non-linearity of the concrete under these loading conditions. A damage model is developed that accounts for the non-linearity as well as different strain rates of the specimens. Both a constitutive model and continuum damage model (CDM) are used for the theoretical analysis. Experimental data is obtained in order to validate the accuracy of the theoretical data, primarily the results of the CDM model.

Although linear elastic models are highly used due to their ease of sophistication; blast loads cause non-linear behavior and therefore render these models incompatible. Constitutive models are used to account for the non-linear behavior that is observed in concrete. Due to concrete's brittle behavior, CDM models have become highly accepted in determining the effects of impact loading in concrete. It follows the basis that deformation causes a degradation of the material that is permanent. Through these models equations can be developed to determine the compressive and tensile strength of concrete under different strain rates. An impact machine is designed to impose an impact load on concrete cylinders. Through this process, the strain rate and stresses are recorded. These results are then compared to the theoretical results obtained from the two models.

When the theoretical and experimental results are obtained and compared, it is found that the experimental values validate those of the theoretical values. Despite such a

simple model, there is an accurate representation of the strength and stress-strain relationship of the concrete. The experimental studies also validated that the higher the strain rate, the initial modulus, compressive strength, and critical strain at maximum stress will all increase as well.

The study conducted by Koh and others (2001) studies both the compressive and tensile strength of concrete under impact loads; however, the shear strength of concrete is not studied. The current study looks to focus on this omission and how the shear strength is effected under dynamic loading. The current attempts to model some of those method developed by Koh and others (2001) to obtain accurate results for the damage effects of concrete under impact loads.

2.1.6 Concrete Properties Subjected to Impact

The rate of strain in a concrete specimen has various effects on the concrete's strength properties. This is tested and confirmed in a test conducted by Suaris and Shah (1983). The high rates of strain can be caused by many factors including but not limited to: missile impacts, blast loads, wind gusts, earthquakes, and ocean waves. During the event of these impact loads, the point of contact undergoes extreme dynamic loading. In order to better design for these loading scenarios, an attempt is made by Suaris and Shah to quantify the effects on concrete. Experimental studies are conducted through a wide range of strain rates to acquire the material strengths and energy absorption through the various strain rates.

In the experimentation conducted, an impact testing system is utilized. A 240 pound striker is dropped onto the specimens to produce the impact loading. Through a series of strain gauges, fiber-optic systems, oscilloscopes, and other data acquisition

devices; response data such as load time and velocity at impact are obtained. The energy absorption trace is then calculated by integrating the load time trace multiplied by the velocity at impact. Flexural tests are also conducted on concrete beam specimens that measure 1-1/2" wide, 3" deep, and 18" long. They span 15" and are loaded at the center with an impact velocity of 40" per second. Neoprene rubber pads are used to obtain two different strain rates and an Instron testing machine obtained three lower strain rates. The energy absorption is calculated by taking the area under the load versus the deflection curve.

Through this testing, Suaris and Shah (1983) determine that the flexural strength of concrete is significantly sensitive to the strain rate. The tensile strength of concrete as a percentage increases the most with an increase in the strain-rate, whereas the compressive strength is the least and the flexural strength lies between the two. This is a result of crack formation and propagation within the concrete matrix and the time it takes for this to occur. A strain rate of 0.67×10^{-6} results in an energy absorption of 0.22 foot pounds (ft-lbs). An increased strain rate of 0.7×10^{-6} results in an energy absorption of 0.35 ft-lbs. This confirms that an increase in strain rate will increase the energy absorption of the concrete.

In this testing; plain concrete, plain mortar, and various fiber reinforced mortars are tested. A concrete mix is selected that results in a compressive strength of 6,930 psi. However none of the testing methods accounted for the effects cause by the shear damage associated with the impact loading. The current study looks at changing the mix designs to see how this affects the concrete's energy absorption. It also test the concrete specimens in shear and observes how this is effected under high frequency impact loads.

2.1.7 Concrete Shear Strengths subjected to Dynamic Loads

In an attempt to evaluate the parameters of reinforced concrete that influence flexural and direct shear under blast loads, Magnusson and others (2014) developed a review of previous literature regarding the subject. Three modes of shear are exhibited under dynamic loads: flexural, direct, and punching shear. However, punching shear is neglected in the review. The main focus of this review looks at quasi-static loading, dynamic shear, and the initial response of concrete elements subjected to dynamic loads.

- Quasi-Static Loading: Before one can understand shear failure in dynamic loading, a quasi-static loading sequence is looked at first. This is a loading in which the load is applied slowly enough that inertial and momentum effects can be neglected. Through this loading, both flexural and shear failure share common features such as the mechanisms that transfer stresses across a crack in the concrete. Those mechanisms are friction, aggregate interlock, and the dowel action of any reinforcement in the concrete. Flexural shear however occurs when there is a combination of both shear and flexural stresses occurring in the concrete. Cracks are initially established due to flexural stresses; however, as the load is increased the cracks propagate vertically. These vertical propagations are more attributed to shear stresses occurring in the member. Direct shear failure typically occurs closer to a support where there is usually a negligible amount of flexural stress on the member. This is more of a sliding type failure that occurs through the entire depth of the element.

- Dynamic Shear: The intensity of a load may cause either of the two shear failure modes previously mentioned. This intensity is a function of the peak loading

as well as how fast the peak load is reached. Due to this time function of loading, a dynamic approach is considered. A blast load causes a near instantaneous peak load causing a dynamic load on the specimen. In beams that were subjected to an evenly distributed blast load over the member, it is found that the flexural shear failure resembles the same properties of a quasi-static load. The roofs of reinforced box concrete structures are tested under blast loads as well. It is found that the roof slabs failed in a direct shear and are completely severed from the vertical walls. It is also noticed that the roofs were relatively flat after failure, denoting negligible flexural stresses in the slab. It can be concluded that shear failure occurs in the early stages of a blast load before there is a chance for large flexural stresses to occur in an element.

- Initial Response of Concrete Elements Subjected to Dynamic Loads: Due to the findings in the dynamic shear section that shear failure occurs in the early stages of a high impulse load, it becomes of interest to study the initial response of the structure. Through this study a simply-supported beam is considered that is subjected to a uniformly distributed along the entire length of the beam. Although researchers have used both the *Bernoulli-Euler* and *Timoshenko* theories of analysis, the *Bernoulli-Euler* method is used in this paper. It is through this analyses that it can be concluded that impulsive loads with a relatively high amplitude can cause a member to fail in shear before it has reached its ultimate shear resistance. Through this findings, one must consider how the initial response of an element may behave to a dynamic load. This instantaneous loading may cause failures that are not expected.

The present study looks at UHPC under high frequency shear. The review conducted by Magnusson and others (2014) is very beneficial in conducting this study. It

aids in determining what factors must be accounted for when determining shear properties of concrete under impact loads.

2.1.8 Driven UHPC H-Piles

The United States will spend approximately $1 billion over the next year in the rehab of deep pile cement foundations. In an attempt to reduce the costs associated annually with these repairs, Suleiman and others (2010) study the possibility of using UHPC as a replacement to normal concrete. It is believed that the UPHC piles will withstand the stresses better not only during service but as well as during the driving of the piles. To verify UHPC as a more effective alternative, the durability, compressive and tensile strengths are examined.

To examine the behavior of UHPC piles, two UHPC HP 10x57 piles are designed. They are driven next to a bridge site near Oksaloosa, Iowa in primarily a loess soil that resides on top of glacial till clay. They are driven with a Delmag D19-42 hammer with a 51-mm thick hammer. Plywood cushioning is used in the driving process to prevent damage to the piles. Once driven, the piles are tested both vertically and laterally. The vertical testing follows standards American Standard for Testing Materials (ASTM) D1143/D1143M-07 Standard Test Methods for Deep Foundations Under Static Axial Compressive Load (ASTM, 2013) and the lateral loading following ASTM D3966-07 Standard Test Methods for Deep Foundations Under Lateral Load (ASTM, 2013). During the driving process, the plywood cushioning disintegrates for both piles before they are driven to the desired depths. They are driven the remainder of the depth without cushioning and it is found that the hammer does not cause any significant damage to the piles, which begins to confirm the durability properties of UHPC. During the lateral

loading of the piles, one of the piles begins cracking and fails sooner than expected. After further observation, it is found that the pile fails at a localized weakness in shear due to 20 mm-thick bundle of instrument wires within the pile. The pile failed at a loading of 101.3 kN, approximately 40 kN lower than what is predicted.

In the testing conducted, the piles are tested vertically first and then tested laterally. In the lateral testing one of the piles fails unpredictably in shear. The shear failure is attributed to the presence of instrumenting wires within the concrete. However it is very possible that due to the vertical loading being tested first, this loading may have cause stress concentrations at the location of the instrumentation. These stress concentrations may cause micro-cracking to occur, and therefore resulting in a lower shear strength. This reduced shear strength in turn caused a shear failure when it was not expected to happen.

The current study examines UHPC and its shear strengths. From the study conducted by Suleiman and others (2010) a UHPC H-pile failed in shear unexpectedly due to instrument wires within the pile. The current study takes note that the slightest imperfections within the concrete matrix can cause unexpected failures. In order to obtain accurate results, the specimens being tested must be uniform, both on the microscopic and macroscopic scale.

2.2 Charpy Impact Testing

2.2.1 Impact Resistance of PVA Reinforced Cementitious Materials

Research has shown that fiber reinforced concrete (FRC) exhibits a higher energy absorption rate than normal strength concrete. A common fiber used in concrete mixtures

is poly vinyl alcohol (PVA) fibers. Poly vinyl butyral (PVB) can also be used as an aggregate replacement in a cementitious mixture. Xu and others (2009) study how using both PVB as an total aggregate replacement and PVA fiber reinforcement effect the energy impact absorption of a concrete mixture and compare it with normal strength and lightweight concrete.

In the process of this study fifteen different mix designs are established. A normal weight concrete, lightweight concrete, and PVB composite concrete are the three base concrete groups. Each base group has four different mix designs: a control, 0.3, 0.6, 0.9 and 1.2 percent volume of PVA fibers, where the control has no fiber component. All mix designs maintain a constant water to cement ratio of 0.4. Charpy impact specimens are molded from these mix designs to conduct the testing. These specimens measure 50.8 mm x 25.4 mm x 25.4 mm. The U-notch created at the center measure 2.5 mm wide by 5.1 mm deep. The general method in the Charpy impact testing follows ASTM E28 Standard Test Methods for Notched Bar Impact Testing of Metallic Material (ASTM, 2014). The specimens are placed in a loading configuration that has supports at 40 mm of the length. The notch is faced towards the outer direction and opposite of the impact surface. A weighted pendulum is raised to a known height. The pendulum is released and impacts the specimen breaking through it. The recovery height is recorded with the machine. The energy absorbed by the specimen is calculated by the height difference times the weight of the pendulum.

It is found through this testing that the PVB composite has the highest energy absorption of an average of 11.00 ft-lb. Normal weight concrete follows with an average impact energy absorption of 8.50 ft-lb and lightweight concrete with the lowest average

value of 7.25 ft-lb. It is also found that for all three groups, the energy absorbed increases as the volume of fibers increase up to 0.9%, after that the energy absorption drops. It is concluded that the addition of the extra fibers reduced the workability and increased the voids in the cement matrix therefore decreasing the energy absorption of the specimens.

This current study follows similar procedures outlined by that of Xu and others (2009). Instead of studying the effects of the addition of PVB composite and PVA fibers on the specimen's energy absorption, this study examines different components of UHPC and how varying the parameters influence the energy absorption. Specimens will be molded in similar manner and the same Charpy impact standard is also followed for this current study.

2.2.2 Parametric Study of Fiber-Reinforced Concrete Subjected to Impact Loads

In the thesis research conducted by Magbool (2012), the impact energy absorption of concrete materials is examined. An approach is taken to optimize the absorption rate through the addition of fiber reinforcement. Both carbon nano fibers (CNF's) and PVA fibers are added to a control mix and their contribution to the energy absorption is studied. Through this process a conclusion is made to improve the impact resistance of fiber-reinforced concrete.

To conduct this study, concrete specimens are first cast and allowed to cure, then subjected to an impact load by means of the Charpy impact testing methods. The specimens are cast in 1" x 1" x 2" plastic molds. They are consolidated by means of a high frequency vibrating table. Once the concrete has been cast for the given mix, a notch is formed in the top of the molds perpendicular to the length of the specimen. The specimens are allowed to cure in the molds for 24 hrs where they are then removed and

placed in lime water baths. They cure in these water baths at room temperature and are tested at 7,14, and 28 days. At these days, the selected specimens are subjected to the Charpy impact testing. The testing methods follow that of standard ASTM E28 (ASTM, 2014). Through this method which also follows that of Xu and others (2009) an impact energy can be found for each specimen.

It is found in this research that the addition of fibers to the cement matrix increases the impact energy absorption, as the hypothesis predicted. The control mix has an average energy absorption of 9.00 ft-lbs. Two different CNF's are tested and they have average energy absorptions of approximately 12 and 13 ft-lbs respectively. The mix containing PVA fibers has the highest absorption rate at approximately 18 ft-lbs.

This current study follows the methodology of both Magbool (2012) and Xu and others (2009). The same molds and Charpy machine utilized by Magbool (2012) are used in this current research. Although the other two researches study the effects of fiber-reinforcement on impact energy, this current study instead studies UHPC and its effect of impact energy absorption.

2.3 UHPC Mix Design and Mechanical Properties

2.3.1 UHPC Technical Specifications

The technical paper furnished by Graybeal (2011) and the Federal Highway Administration (FHWA), provides an overall examination of UHPC. This investigation includes a definition of UHPC, its applications, availability, mixing and casting procedures, curing procedures, testing procedures, sample preparation and extraction, structural design analysis and modeling, and finally how to inspect UHPC. All of these

areas are not only examined in the report, but they are also compared to normal weight reinforced concrete.

UHPC is defined as a concrete mixture with: a water to cement (w/c) ratio of less than 0.25, a compressive strength of 21.7 ksi, and a post-cracking tensile strength of 0.72 ksi. UHPC is currently used in pre-stressed girders for three different bridges in the United Sates. There are additional investigations to use UHPC in precast concrete piles, seismic retrofit of bridge substructures, overlays for bridge repair, and security and blast mitigation applications. There are approximately five commercially available products available in Europe with one of them an international propriety product available in the United States. The developing interest of UHPC however, has caught the attention of other producers as well as an increase in research programs in both Europe and the United States to produce UHPC from locally available material.

The mixing and casting of UHPC is extremely similar to that of normal weight concrete. The biggest difference being the energy input required for UHPC mixing is greatly increased. Due to the lack of coarse aggregate, a low w/c ratio, and the increased energy, additional measures are to be taken to ensure the UHPC does not overheat during mixing. It is important in the curing of UHPC to seal the specimen to prevent any loss of water. The specimens should be cured at a higher temperature than normal weight concrete and if possible, utilize the use of steam treatment as well.

Testing of UHPC is very similar to the procedures for normal weight concrete as well. The variations occur however due to the increased strengths of the UHPC. Typically to mitigate these issues, smaller sample sizes are used in the testing procedures. The flow of UHPC is measured by ASTM C1437 Standard Test Method for Flow of

Hydraulic Cement Mortar (ASTM, 2015) as opposed to the typical slump test of normal weight concrete to measure the mix quality. Compression testing follows ASTM C39 Standard Test Method for Compressive Strength of Cylindrical Concrete Specimens (ASTM, 2015) and C109 Standard Test Method for Compressive Strength of Hydraulic Cement Mortars (Using 2-in. or [50-mm] Cube Specimens) (ASTM, 2016) with the only variation being an increased load rate of 150 psi/s. Modulus of elasticity follows ASTM C469 Standard Test Method for Static Modulus of Elasticity and Poisson's Ratio of Concrete in Compression (ASTM, 2014) without any changes to account for UHPC. Chloride penetration tests follows AASTHO T259 Standard Method of Test for Resistance of Concrete to Chloride Ion Penetration (AASTHO, 2013) and ASTM C1202 Standard Test Method for Electrical Indication of Concrete's Ability to Resist Chloride Ion Penetration (ASTM, 2012) standards with no major discrepancies. Freeze-thaw durability tests currently follow ASTM C666 Standard Test Method for Resistance of Concrete to Rapid Freezing and Thawing (ASTM, 2015). Due to the low w/c ratio, when the specimen is exposed to water, it may absorb additional water, resulting in inflated results from the actual performance of the UHPC.

The preparation of UHPC samples follow the same methods as those used in normal weight concrete. Cutting and grinding equipment also proves to be applicable in the preparation of UHPC specimens. In the design, analysis, and modeling of UHPC, basic engineering fundamentals still apply. In analysis of UHPC, it is imperative however to not allow biased notions to fog computations. It must be analyzed as a separate entity that does not behave the same as normal weight concrete. Inspections of UHPC follows the same methods as those of normal weight concrete. The cracking in UHPC however is

much smaller and sometimes may not be seen by the naked eye. Advancing technologies are used to aid in the inspection of UHPC to determine the performance and its durability.

As the availability and studies of UHPC continue to advance, it is important that the understanding of the material's properties advances as well. Knowing how it relates to normal weight concrete has given a foundation for the behavior of UHPC. With this knowledge, the applications of UHPC will continue to grow. This current study utilizes the information provided by Graybeal (2011) to study the energy absorption of UHPC and its effectiveness in shear strength.

2.3.2 Testing Methods for UHPC

Due the high compressive strengths of UHPC, property testing procedures to obtain the compressive strengths can be quite challenging. With such high compressive strengths, testing machine capacity and cylinder end preparation can be ineffective in properly testing UHPC specimens. Due to the compressive strength of concrete being the mechanical property that verifies the mix's acceptability, the importance to accurately determine this is becoming crucial. Graybeal and Davis (2008) develop a study to establish the most accurate and precise method to determine the compressive strength of a concrete mix.

In order to determine the most accurate way to test a concrete mix, Graybeal and Davis (2008) study the effects of using different size cubes vs. different size cylinders in testing procedures. The different size cylinders tested are 2, 3, and 4 inch cylinders as well as 2, 2.78, and 4 inch cube specimens. Three different mix designs are used in this testing that have compressive strengths ranging from 11.6 – 29 ksi. The cylinders are tested according to ASTM C39 (ASTM, 2015) and the cubes to ASTM C109 (ASTM,

2016). The only deviation from these standards is the initial load application is increased to 150 psi/second for the testing of both cylinders and cubes. They are all tested in 1000 kip compression testing machine.

After the testing is concluded, trends are found in the results. The 2.78 and 2 inch cubes show very similar strengths with their confidence intervals overlapping. The strengths of these specimens tend to be at or above the other specimens. The 4 and 3 inch cylinders show similar strengths with most of their confidence intervals overlapping. The 2 inch cylinders show similar to lower strengths compared to the other specimen types. It is also determined that mixes lacking fiber reinforcement display higher coefficients of variation.

The current study looks at the compressive strength; along with other mechanical properties of UHPC, and therefore benefits from the information provided in the study by Graybeal and Davis (2008). With a compressive machine with a load capacity of 300 kips, and the lack of expensive end preparation equipment, other methods are necessary to accommodate the available testing setup. The conclusions presented by Graybeal and Davis (2008) make this current study feasible with accurate results.

2.3.3 UHPC Using Local Materials

Due to the increased use of UHPC, Allena and Newtson (2010) conduct a study to produce UHPC using only local materials. Conceiving a mix design that uses only local materials provides for a number of advantages. It decreases the cost of the mix from commercially available products, the sustainability is improved, and the mechanical performance rivals that of those commercial products. It is found through their research

that mix designs can be produced using local materials having compressive strengths up to 23,000 psi.

In the development of a UHPC, Allena and Newtson (2010) design a mix that contains only a Type I/II Portland Type cement, fine quartz sand, silica fume, steel fibers, and a high range water reducing admixture (HRWRA) with a polycarboxylate-base. The lack of a course aggregate enriches the homogeneity of the mix. This also allows for a more compact dense mix. Seven different mix designs are developed, some of those contain steel-fiber reinforcement while others don't. Compressive strength specimens are tested using 2" cubes and 4" x 8" cylinders. They are tested according to ASTM standard C39 (ASTM, 2015). Modulus of rupture testing utilizes 3" x 4" x 16" prisms and are tested to ASTM C78 Standard Test Method for Flexural Strength of Concrete (Using Simple Beam with Third-Point Loading) (ASTM, 2015). Three different curing regimes are used to cure the UHPC samples.

Through this process, Allena and Newtson (2010) are able to produce a mix design that produces a UHPC with local materials. One mix design has a compressive strength ranging from 15.2-17.1 ksi, where a second mix design ranges from 17.7-23.5 ksi; both are dependent on the curing regime. It is concluded that the strengths of the mix designs produced with local materials are comparable to commercial products such as Ductal®. The current study uses those mix designs developed by Allena and Newtson (2010). The development of UHPC using local materials allows for the ability to carry out a parametric study on the mix design.

Allena and Newtson (2010) test for both the compressive strength and modulus of rupture for their given mix designs, however; a test on the mix's shear strength has not

been conducted. Due to this omission, the current study focuses on the shear strength for those mix designs developed.

2.3.4 Mechanical and Durability Properties of UHPC

The research conducted by Allena and others (2011) develops procedures to produce UHPC and its corresponding mechanical properties and durability. When certain fundamental principles are followed, a UHPC with improved strength and durability is obtained. When compressive strengths start to approach 20 ksi, the weak link of a concrete mix becomes the course aggregate. The removal of course aggregate then eliminates the weak link and these strengths are achieved. A low water to cement ratio is also manipulated through the use of superplasticizers to furthermore increase the compressive strength of concrete. Allena and others (2011) look at those principles required for UHPC and previous literature in the development of UHPC.

Some of the most basic principles that are suggested by Allena and others (2011) as well as other authors are as follows:

- Remove the course aggregate.
- Reduce the water to cement ratio.
- Create a pozzolanic reaction through the use of silica fume.
- Heat treat samples to improve the microstructure's mechanical properties.

As mentioned previously, removal of the course aggregate removes the weak link in UHPC. The maximum aggregate size recommended by Allena and others (2011) is 0.026 inches. In concrete mix design, the controlling factor of compressive strength is the w/c ratio. Reducing this ratio to a minimum will result in a maximum compressive strength. The pozzolanic reaction is a chemical reaction within the cement matrix that

increases the cementitious bond properties of the microstructure. This reaction is also enhanced when the cement is cured under heat treatments. Allena and others (2011) test the various UHPC properties under various curing conditions and then compare them to research of other publications.

It is found through this research that UHPC has exceptional properties and compares to previous testing results. The compressive strength of UHPC far exceeds that of normal weight concrete. The flexural strength, modulus of elasticity, shrinkage-swell behavior, water absorption, chloride penetration, and freeze-thaw durability properties of UHPC all prove to have surpass those of normal weight concrete. All of the previous mentioned properties were tested by multiple publications and shown to have similar results. However, of those mechanical properties, the shear strength of the UHPC has yet to be tested. This current research will look at UHPC and how the shear strength is effected by different properties of the UHPC.

2.3.5 Durability of UHPC

In the study conducted by Graybeal and Tanesi (2007), the durability of UHPC is examined. Different curing treatments of a commercially available UHPC are applied to concrete samples to better understand their durability. The focus is on a steam treatment in anticipation that it will increase the hydration of the concrete; therefore improving its microstructure and decreasing the permeability.

The UHPC studied is commercially available in the United States known as Ductal®. The mix contains fine sand, cement, silica fume, and steel fibers. The samples are tested under four different curing regimes; 3 of which include steam treatment and the 4^{th} curing condition is an untreated curing condition that cures in a standard laboratory

environment. The durability properties to be tested and their corresponding testing standard are:

- Chloride Ion Penetration - ASTM C 1202 (ASTM, 2013) and AASHTO T259 (AASHTO, 2013)
- Scaling Resistance – ASTM 672 Standard Test Method for Scaling Resistance of Concrete Surfaces Exposed to Deicing Chemicals (ASTM, 2012)
- Abrasion Resistance – ASTM C 944-99 Standard Test Method for Abrasion Resistance of Concrete or Mortar Surfaces by the Rotating-Cutter Method (ASTM, 1999)
- Freeze Thaw Degradation Resistance – ASTM C 666 (ASTM, 2015)
- Alkali-Silica Reaction (ASR) – ASTM 1260 Standard Test Method for Potential Alkali Reactivity of Aggregates (Mortar-Bar Method) (ASTM, 2014)

All tests follow the four curing regimes with the exception of the Alkali-Silica Reactions, which are altered due to the timetable allotted by ASTM 1260 (ASTM, 2014) that does not coincide with the previously defined curing regimes.

Through a series of 5 tests, it is found that the durability of UHPC far exceeds that of normal strength concrete. It is found through the Chloride Ion Penetration that the penetrability for all regimes range from negligible to very low. All four curing regimes result in very little to no scaling issues according to the given standard. The three treated curing regimes have a much higher abrasion resistance as compared to the untreated

regime. Despite the curing regime, UHPC is extremely freeze-thaw resistance. And lastly, ASR has negligible effects to UHPC under any of the four curing regimes.

Although this current study does not account for any durability properties of UHPC, the study conducted by Graybeal and Tanesi (2007) assist in detailing how curing regimes affect the microstructure of UHPC. In taking this into account, curing regimes can be modified to produce a higher shear strength UHPC mix. However Graybeal and Tanesi (2007) only look at a UHPC that has steel fiber reinforcements, whereas this study looks at UHPC that doesn't contain any steel fibers.

2.3.6 Mechanical Properties of UHPC

To obtain a better comprehension on the mechanical properties of UHPC, Prem and others (2012) conduct their own study of UHPC. In designing a mix that contains only cement, fine sand, silica fume, steel fiber reinforcement, quartz powder, superplasticizer and a low water to cement ratio, a UHPC can be obtained and its properties studied. It is through these studies that the commercialization of UHPC for structural applications will be soon be achievable.

For the purpose of this study Prem and others (2012) investigate multiple mechanical properties of UHPC. The UHPC mix is first cast using local materials in a planetary mixer. The dry materials are first mixed then the water and superplasticizer are gradually added in later in three different intervals. The specimens cast are 100 x 100 x 100 mm cubes, 100 mm diameter by 200 mm tall cylinders, and 70 x 70 x 350 mm beams. They are allowed to cure for 24 hours and then placed in their respective curing regime. The curing regimes consists of a combination of either/or ambient air curing,

water curing, and hot air curing. To determine the mechanical properties a corresponding testing standard is followed:

- Compressive strength - ASTM C109 (ASTM, 2015)
- Tensile strength - British Standard (BS) 12390 Testing Hardened Concrete. Tensile Splitting Strength of Test Specimens. (BS, 2009)
- Flexural strength - ASTM 1609 Standard Test Method for Flexural Performance of Fiber-Reinforced Concrete (Using Beam With Third-Point Loading) (ASTM, 2012)
- Water absorption – ASTM C 642 Standard Test Method for Density, Absorption, and Voids in Hardened Concrete (ASTM, 2013)
- Rapid chloride penetration test - ASTM C 1202 (ASTM, 2013)

It is found through compression testing that the samples obtain 90% of their compressive strength after 14 days of curing. Regardless of the aspect ratio of the steel fibers, the compressive strength increased by 25% over those mixes without the addition of fibers. The addition of fibers also prove to increase the tensile strength of the UPHC. As the reinforcing index of the mix decreased, the flexural strength of the mix decreased as well. It is determined by the water absorption rate and the rapid chloride penetration test that the UHPC allows for a very high corrosion resistance

Some of the mechanical properties investigated by Prem and others (2012) are also examined in this current study. Those methods are modeled to provide for accurate results for this given study. Prem and others (2012) however researched the mechanical properties that steel fiber reinforcements provided to UHPC. This current study

investigates the mechanical properties of the UHPC constituents without the use of those fibers. This current study also examines the impact energy absorption and shear strength of UHPC where Prem and others (2012) did not.

2.3.7 UHPC: A Simpler Way

In a study conducted by Wille and others (2011), methods are developed to produce a UHPC that can be derived from local materials and not require special equipment or treatment in the process. It is the belief of the researches that if the packing density of the cementitious mixture is increased then a UHPC can be easily attainable. Through different methods of study, a mix design is optimized for the maximum attainable compressive strength of the concrete mix.

The first thing in optimizing the UHPC mix is insuring a low porosity and therefore maximizing the packing density. This is achieved by testing the paste of each mix according to ASTM C230/C230M Standard Specification for Flow Table for Use in Tests of Hydraulic Cement (ASTM, 2014). The paste is the cementitious mixture without the addition of any aggregate/sand. The larger the spread signifies less voids and air entrapped in the mix and therefore a higher compressive strength. Different mix designs are tested using varying w/c ratios, type of cement, type of silica fume, powder proportions, and influence of HRWR in the paste. Once an optimized paste is selected, sand is then added to the mix and tested for compressive strength for final evaluation.

Each parameter is studied independently and used to optimize the paste mix. It is found through the spread that a w/c ratio of 0.22 has the optimal spread for the mix. The type of cement used to best achieve a high strength mix is a Type I Portland cement with low content of C_3A and a fineness modulus of approximately 281,000 in^2/lb. The type of

silica fume used is found to be negligible but is required to achieve high strengths. The proportioning of powders is found to have a negligible effect on compressive strength, but optimizing the proportion can increase the spread value. Lastly the type and amount of HRWR is found to have an ideal rang of 1.4%-2.4% of the cement by weight. An optimum sand to cement ratio in this study is found to be 1.4.

The study by Wille and others (2011) is important in producing an UHPC using local materials, especially for the current study that generates a UHPC in the same manner. This current study uses some of those methods provided by Wille and others (2011) to create its own UHPC. However, Wille and others (2011) neglect to account for curing conditions in the production of their UHPC. This current study accounts for different curing conditions and their effect on the mechanical properties of a UHPC.

2.3.8 Mechanical and Durability Properties of UHPC

In a study conducted by Magureanu and others (2012), UHPC is studied under different curing conditions and the resulting properties of the concrete are analyzed. It is stated by the authors that UHPC must have a compressive strength of 21,756 psi and tensile strength of 1015 psi. The properties that are investigated of the concrete mixes are compressive strength, static and dynamic modulus of elasticity, splitting and flexural tensile strengths, and the freeze-thaw resistance. The mix design of the UHPC utilizes local resources; which in turn, provided exceptional mechanical properties and durability.

In the testing of the UHPC, two different mix designs are used; one mix design containing hybrid steel fibers while the other one is without. The mix design without fibers consists of 1 part cement, 0.259 parts Silica Fume, 0.125 w/c ratio, 0.69 parts quartz sand, and 0.065 HRWRA. The mechanical properties are tested on specimens at 6

days of curing; 5 of those days in a steam cure of 194° F and 80-90% relative humidity. Compressive and splitting tensile strengths are tested in accordance with standards EN 12390-3[9] and EN 12390-6[10] respectively on 3 different sizes of cubes. While the flexural tensile strength in accordance with EN 12390-5[11] on two different prism sizes.

In the testing of the cubes for both their compressive strength and splitting tensile strength, it is found that the strengths for both dropped as cube sized increase. For cubes of 1.97 in on each side, the compressive strength is 22,771 psi and a tensile strength of 1,168. As cube sizes are increased to 3.94 in, the compressive strength drops to 17,840 and the tensile strength to 686 psi. All values coming from the mix design not containing any fibers. The same trend is seen for the flexural strength with the smallest prism (1.57 x 1.57 x 6.29 in) having a strength of 2020 psi dropping to 1363 psi for a prism size of 3.94 x 3.94 x 11.81 in. Having classified UHPC as a cementitious composite with compressive strength of 21,756 psi and tensile strength of 1015 psi; only the smallest samples could be considered UHPC under this standard.

The current study uses UHPC and tests the shear strength of the mixes. This study conducted by Magureanu and others is a strong basis on the mix design and design procedures to obtain a UHPC mix. It will be noted that in general the size of the specimens and strengths are inversely related. This is valuable to know when the specimens are cast for the current study.

As stated, the strengths of the concrete mixes overall did not reach the values required to be classified as UHPC. Normally the strength of concrete is tested at 28 days, where in this research done by Magureanu and others (2012) the early strength was tested at 6 days. Waiting the full 28 days could possibly give the desired strengths. The

specimens are also cured under only one curing condition for the short term strengths. Different curing conditions can be sought to obtain higher strengths for the concrete.

2.3.9 Optimal Conditions for UHPC

With the increasing popularity of UHPC around the world, Tam and others (2009) research the feasibility of utilizing it within the Hong Kong area. This study aims to optimize the compressive strength of UHPC or what they call reactive powder concrete (RPC); as well as the practical and economic benefits. The parameters studied are the fine sand gradation, water-to-binder ratio, superplasticizer dosage, and curing conditions.

The production of the UHPC is all from local materials available to the study. The testing of the samples are in accordance with BS 1881: Part 116, 117, and 121. Water to binder ratio is tested at a ratio as low as 0.17 and as high as 0.40. To determine the effects of superplasticizer it is taken as a percentage of the cement by weight and ranges from 2%-3.5%. The effect of the gradation of sand is grouped into four factions and those are ranges of: 150-300 μm, 150-600 μm, 600-1180 μm, and 150-600 μm. Three different curing regimes are tested at differing water temperatures and curing environments. Lastly the effect of the heating regime is tested in six different regimes of different temperatures and the duration of those temperatures. All tests are performed and recorded as well as each sample's microstructure is monitored under a scanning electronic microscope (SEM) to assist in providing clarity of the results.

Through this parametric study, Tam and others (2009) believe to have found optimum conditions for a UHPC. It is found that the water-to-binder ratio of 0.2 to be the most optimum ratio for compressive strength. Enough water is provided for complete hydration of the cement, but no so much that the water provides for weak air pockets

within the cement matrix. The prime amount of superplasticizer in a mix is found to 2.5%. Additional superplasticizer increases the workability, however it does not increase the compressive strength and requires longer curing for initial settlement. Through the studies it is found that the optimal gradation size is the group of 150-600 μm. This provides large enough particles to provide for strength but also small enough to fill voids and achieve a large packing density which is essential to compressive strength. The testing shows that increased temperatures have a significant impact on increasing compressive strength of UHPC, however the duration of these temperatures seem to be negligible.

As in the study conducted by Tam and others (2009), the current study carries out a parametric study on UHPC. Therefore, the current study will utilize some of those optimized results from Tam and others to produce a UHPC to be studied. The research conducted by Tam and others studies the compressive strength, split tensile strength, and modulus of elasticity. However the shear strength is not studied; consequently the current research attempts to optimize the shear strength properties of UHPC.

2.3.10 Strengths of UHPC Under Variable Curing Conditions

The use of UHPC in structures is becoming much more prevalent in today's society. Its high compressive strength is very appealing in the design process. However due to the minimal knowledge of UHPC's characteristics and properties, there aren't the standard tests used by ASTM and AASHTO that is used in normal-strength concrete. Ahlborn and others (2011) recognize this need for newer standards and testing procedures to verify previous claims about the strength and durability of UHPC. Laboratory tests are

conducted on concrete specimens to help verify some of these claims and further the knowledge of UHPC.

Ahlborn and others (2011) look at many different properties of UHPC and how curing the specimens will affect those properties. For all tests, the specimens are mixed with a high shear capacity mixer, along with a vibratory table and cure at a relative humidity of 100% and at a temperature of 194° F in a steam cure chamber. The different curing regimes utilized are an ambient air curing, 48 hour thermal steam treatment (TT), delayed thermal steam treatment: 10-day delay before curing is applied (DTT), and double-delayed thermal steam treatment: 24-day delay before curing is applied (DDTT). Different samples are tested to characterize how the curing conditions have on their compressive strength, modulus of elasticity, Poisson's ratio, flexural strength at first crack, rapid chloride penetration, freeze-thaw durability, and coefficient of thermal expansion. All tests follow the corresponding ASTM standard with a few having justified variations.

Through the testing conducted by Ahlborn and others (2011), it is found that curing conditions affect some parameters of UHPC while others it has no effect. For the compressive strength of the UHPC, the specimens subjected to thermal treatment all experience a greater strength than those cured in the air; however, the three different thermal regimes don't show any significant difference. The same trend is noticed in terms of the modulus of elasticity with a greater modulus for those cured under thermal treatment. In testing of Poisson's ratio, it is found that the curing regimes didn't have an effect and results were similar for all cases. The flexural testing findings have different results for each curing regime with no obvious trend and also has the largest coefficient

of variation for all properties tested. It is found through the rapid chloride penetration tests that the tested specimens for both air and TT regimes pass the ASTM standard with the TT samples having better results. It is found that specimens that are thermally treated in both freeze-thaw cycles as well as wet-dry cycles slightly increased in relative dynamic modulus but air-cured specimens had a much higher increase for the same two cycles. This relatively small change in relative dynamic modulus shows a higher resistance to the effect due to freeze-thaw conditions. In testing the coefficient of thermal expansion, it is found that the UHPC cured thermally changed very little when tested at 7 and 28 days. This indicates that the UHPC properties are essentially secured after treatment has occurred.

In examining the shear strengths of normal concrete and UHPC, the curing conditions are vital in ensuring consistent specimens. The study by Alhborn and others (2011) can be used to model curing conditions to ensure a consistent specimen sample that will give the best results in the shear testing. Overall it is found that thermal treatment of the test specimens provided the best results and may be imitated.

This study looks at how curing regimes affect different properties of UHPC. Although it looks at air curing and thermally curing specimens, it neglects to look at curing the test specimens in a water bath. This method is very common in curing concrete specimens which maintains a high water to cement ratio. This ratio is crucial in the curing of concrete and the resulting properties of a specimen.

2.4 Conclusions

This literature review provides for an insight on previous research relevant to this study. The three main topics focused on providing for the information required to conduct this study. From this literature review a few key points are taken.

1. Macroscopic studies show that structures under high intensity short duration loading (impact/blast loads) typically fail in shear.
2. These shear failures have not been studied however on a microscopic scale.
3. The impact/blast loads can be closely modeled under Charpy impact testing methods and the energy absorption can be captured.
4. Due to UHPC being a relatively new concept, not all the mechanical properties have been determined. Shear strength of UHPC has not been studied and therefore the properties are unknown.
5. UHPC mix designs are obtainable through the use of local materials. In using local materials, a parametric study is feasible to determine the mechanical properties most sensitive to energy absorption and shear strength of UHPC.

These key points outline the necessity of this study. They then begin to lay the foundation for the methodology that will be utilized to address the objectives of this study.

CHAPTER 3

METHODOLOGY

3.0. Introduction

During the testing carried out in this thesis, there are multiple testing procedures and ASTM standards which are followed. A mix design using local materials is first obtained to meet compressive strength standards for Ultra High Performance Concrete (UHPC). Once a mix design is acquired and designated as the control mix design, parameters such as water-to-binder ratio, percent silica fume replacement, and gradation effect of the silica sand will be altered to carry out a parametric study of the compressive and energy absorption properties of UHPC. These properties are tested by means of compression and Charpy impact absorption, along with each parametric change. The obtained results from the parametric studies are compared to determine each constituents contribution to UHPC's compressive and energy absorptive behavior.

3.1. Mix Design

In order to change parameters within the mix design, a control mix design is first found using locally available materials. The cement used in this study meets ASTM C-150 Standard Specification for Portland Cement (ASTM 2015); for Type II-V cement and is supplied by Ash Grove Cement Company. The silica fume is Rheomac SF 1000 – Dry Densified Silica Fume and is supplied by BASF. The High Range Water Reducer (HRWR) is MasterGlenium 3030 and is also supplied by BASF. MasterGlenium 3030 meets ASTM C 494/C 494 M Standard Specification for Chemical Admixtures for Concrete (ASTM 2015); requirements for Type A water-reducing and Type F, high-range water-reducing admixtures. The fine sand is an industrial quartz with a grade of 4060

(60% retained on the 40 mesh or coarser) and is supplied by Rocky Mountain Supply. This sand is passed through a number 30 sieve to control the particle size of the sand. The material specifications for each constituent can be found in Appendix A.

In order to determine a control mix, five different mix designs are tested. Along with these mix designs, different mixing and casting methods are investigated as well. At the conclusion of testing these mix designs and methods, it is determined that a mix design suggested by Allena and Newtson (2010) will function as the control mix for this study. This mix design provides the highest compressive strength and can be categorized as a UHPC. The mixing methods used for this mix are detailed later in this section. The other mix designs evaluated, but not chosen, can be found in Appendix B. This mix provides the highest compressive strengths and ultimately coincides the best with the local materials used. This mix design is shown in Table 3.1. All constituents with the exception of the High Range Water Reducer (HRWR) are specified in a lb/yd^3 dosage. The manufacturer for HRWR prescribes the superplasticizer to be measured by volume as opposed to weight, therefore it is specified as $gallons/yd^3$.

Table 3.1: Control Mix Design

	lb/yd^3
Cement	1500
Silica Fume	375
Fine Sand (pass through #30)	1411
Water	375
HRWR (gal)	6

In observing the control mix, certain constituents are identified to be altered for the parametric study. The first parameter identified is the silica fume replacement. Silica fume serves multiple purposes within the concrete matrix and is therefore deemed appropriate for the study. In changing the percentage of silica fume, the effects on the cement are acquired. To determine those effects, it is decided that the silica fume is to be both increased and decreased by 5% and 10% by weight from the control amount.

The second parameter to be changed is the water to cement (w/c) ratio. This is the ratio of water to both cement and silica fume. General concrete mechanics state that the w/c ratio and compressive strength are inversely proportional; however, the effects of w/c ratio on energy absorption in UHPC is unknown. Therefore this parameter is also selected for the study and the water to cement ratio is both increased and decreased by 2.5 and 5% by weight from the control amount.

The final constituent selected from the control mix is the quartz sand. As opposed to the previous two parameters that focus on the percent composition, this parameter focuses on the quality of the constituent. The quartz sand is sieved through the #30 sieve for the control mix. For the parametric study, one mix uses only sand that has been retained on the #30 sieve and the other mix has a 50/50 blend of both passing and retained on the #30 sieve. These two mixes have the same proportions by weight as the control mix with the only difference being the gradation of the fine sand.

Table 3.2 illustrates the ratios required to meet the various parametric mixes stated previously. These ratios are based off the control mix design shown in Table 3.1. For the water parameters, the total water is increased and decreased by 10% and 20%. Varying the water amounts by these percentages alters the w/c ratio by ±2.5% and ±5%.

The HRWR is also either increased or decreased to compensate for the change in water using the manufacture's recommended dosage. The same process is followed in the silica fume mixes. As the silica fume is decreased, the cement is increased; this alters the cement content and therefore the w/c ratio. This is done to keep the w/c ratio the same as the control mix design. For each mix design nine 2 inch x 2 inch cubes for compression and 12 Charpy samples are cast. The actual weights for each mix design can be found in Appendix B.

Table 3.2: Parametric Ratios

	Cement	Silica Fume	Fine Sand	Water	HRWR
Control	1	1	1	1	1
Water 1	1	1	1	1.2	0.95
Water 2	1	1	1	1.1	0.975
Water 3	1	1	1	0.9	1.025
Water 4	1	1	1	0.8	1.05
Silica Fume 1	1.05	0.8	1	1	1
Silica Fume 2	1.025	0.9	1	1	1
Silica Fume 3	0.975	1.1	1	1	1
Silica Fume 4	0.95	1.2	1	1	1
Sieve 1	1	1	100% retained on #30	1	1
Sieve 2	1	1	50/50 blend	1	1

Depending on the size of the batch to be cast, the UHPC is either mixed in a barrel mixer for larger quantities as shown in Figure 3.1 or in an industrial food mixer for smaller quantities shown in Figure 3.2.

Figure 3.1: Barrel Mixer

Figure 3.2: Food Mixer

The procedure used to mix the UHPC is as follows:

1. Mix the quartz sand, cement, and silica fume together. Mix for approximately five minutes to ensure a well graded mix.
2. Add the water while the mixing apparatus is running. This prevents coagulation of the cement matrix therefore reducing mixing time. Mix for approximately five minutes.

3. Add the superplasticizer once again while the mixing apparatus is running. Allow concrete to mix anywhere from thirty minutes to an hour and a half. This time is dependent on the size of the batch and the mix design. Mixing ceases when the concrete reaches a workable state and can be cast into the molds.

When the samples are done mixing they are cast into their respective molds. The casting procedures are outlined in Section 3.2. The specimens are left in their molds at room temperature for 24 hours. The following day after they are removed from their molds, they are placed into their curing regime. All samples are cured in a lime water bath that is held at a constant temperature of 50° ± 1.5° C. This temperature is maintained in a Caron Freeze/Thaw Chamber as shown in Figure 3.3.

Figure 3.3: Caron Freeze/Thaw Chamber

The final two days of curing, the samples are removed from the water bath and placed in an oven at a constant temperature of 200° C. The heat curing is important in the production of UHPC to establish the pozzolanic reaction from the silica fume. This

chemical reaction is necessary to obtain the high compressive strengths associated with UHPC.

3.2 Casting of Specimens

3.2.1 Cube Casting

For the compression testing of concrete samples, ASTM C192 Standard Practice for Making and Curing Concrete Test Specimens in the Laboratory (ASTM 2015) standard is typically followed using either 4 inch diameter by 8 inch tall or 3 inch diameter by 6 inch tall cylinders. In order to achieve accurate results, the cylinders are capped using a sulfur based compound. However the capping compound is only rated up to approximately 10,000 psi. With such high UHPC strengths, a different method is required to test the compressive strength of the mix design.

To accomplish this, the cylinders are replaced by 2 inch cubes and cast according to ASTM C109 Standard Test Method for Compressive Strength of Hydraulic Cement Mortars (Using 2-in. or [50-mm] Cube Specimens) (ASTM 2011). The cubes are cast in cubic metallic molds and follow similar procedures to those of cylindrical specimens. The molds used can be seen in Figure 3.4. The molds are first lubricated using WD-40 to ensure that the concrete doesn't stick to the molds and allow for a simple removal. The molds are filled 1/3 of the volume at a time and then rodded 25 times for each lift. Once the molds are filled and rodded in three lifts, the tops are troweled to provide for a flat uniform surface on the top. Typically 4 inch cubes are recommended by Graybeal and Davis (2008) for this method, but accurate results can be obtained from the 2 inch cubes by increasing the number of specimens. Therefore nine cubes are cast for each mix

design to test the compressive strength of the mix. The specimens are left in their molds for 24 hours and then removed and placed in the curing regime as previously stated.

Figure 3.4: Cube Molds

3.2.2 Charpy Impact Casting

The specimens that are cast for the Charpy impact testing are 1inch x 1inch x 2inch specimens. The mold used can cast up to 18 specimens at one time and is shown in Figure 3.5.

Figure 3.5: Charpy Impact Molds

Due to the small size, the mold is filled in only two lifts but is still rodded 25 times for each lift. Once the mold is filled the notch is created in the top of the specimen with the top piece also shown in Figure 3.5. After the notch has been created a trowel is used to flatten the top surface. The piece used to create the notch is left in the specimen while it cures in the mold for the first 24 hours. After curing in the molds for 24 hours, they are removed and placed in the curing regime as stated previously. An example of a finished Charpy specimen can be seen in Figure 3.6.

Figure 3.6: Charpy Specimen

3.3 Charpy Impact Testing

The Charpy V-notch Impact Testing is a relative testing method and doesn't give absolute values. However, for the sake of the parametric testing, it suffices in testing the impact energy absorption and shear strength of the different mix designs. The Charpy impact machine used in this study is shown in Figure 3.7.

Figure 3.7: Charpy Testing Machine

As the head is dropped from a known height, it impacts the specimen at a high speed and high strain rate. This provides for an impact that models a blast load on the concrete. The specimen is placed with the notch to be facing outwards as shown in Figure 3.8.


Figure 3.8: Charpy Testing Setup

This provides for a weak spot for the specimen to break. The law of the conservation of energy states that if a pendulum is dropped from a known height it will return to that same height on the opposing side assuming no losses. Consequently, when the pendulum strikes the specimen it will lose energy to the impact and breaking of the specimen. This energy loss can be obtained from the scale seen in Figure 3.9. Each Charpy specimen is subjected to the test and the energy absorption is recorded.

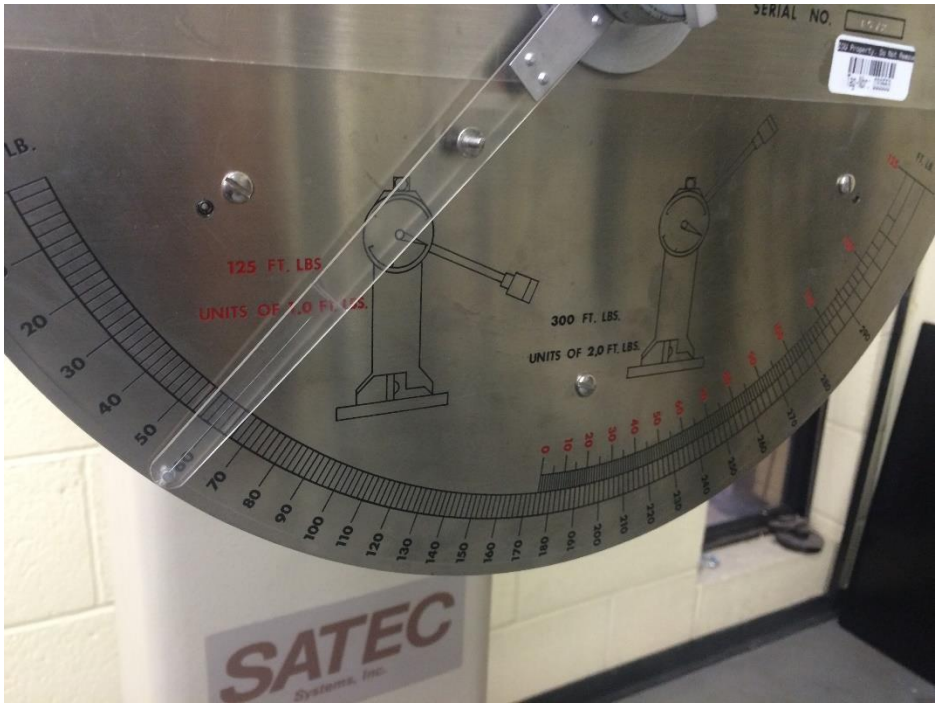

Figure 3.9: Charpy Scale

3.4 Compression Testing

For the compression testing of the specimens, ASTM C109 is followed. As mentioned in Section 3.2.2, the specimens will cure for twenty eight days prior to testing. At the time of testing, the specimens' width, length, and height are measured to find the cross-sectional area and volume of each specimen. Once measured the specimens are placed in the loading apparatus one at a time with the troweled (top) face turned to the

side as to not be in the loading platen. The loading apparatus is a 300 kip capacity Gilson Compression Machine shown in Figure 3.10. The specimens are placed in the machine where both top and bottom surfaces are wiped down with a layer of lubricant; in this case WD-40 is used. This testing setup can be seen in Figure 3.11.

Figure 3.10: Gilson Compression Machine


Figure 3.11: Compression Testing Setup

The loading apparatus is configured to continually capture the applied load on the specimen. A load of approximately 150 psi/second is applied to the specimen as

suggested by Graybeal and Davis (2008). Once the specimen is no longer withstanding a load and has dropped below 25% of the max load applied, the test will cease and the max load is displayed. After the test has terminated, the digital screen displays the peak load, peak stress, current load rate in pounds per second, and the input specimen size. An example of this digital readout can be seen in Figure 3.12. This load is used along with the measured cross-sectional area of the cube to determine the compressive strength of the UHPC.

Figure 3.12: Gilson Digital Screen

CHAPTER 4

LABORATORY TESTING RESULTS

4.0 Introduction

The results for this thesis are obtained through the methodology presented in Chapter 3. For laboratory testing procedures, nine compression samples and twelve Charpy impact specimens are cast for each mix design. Prior to testing, each specimen's dimensions are measured nine times; three measurements each for the width, depth, and height. These measurements are used to calculate the strengths of the specimens respective to the test being conducted and is further explained in this chapter.

This chapter is divided into three main sections: compressive strengths, energy absorption rates, and a correlation between the two strength parameters. The first two sections include average values as well as the related standard deviation and coefficient of variation results for each parametric mix design. The final section presents a comparison between compressive strength and its associated energy absorption rate. Complimentary testing results for individual specimens can be found in the Appendices C and D. Using the results obtained in the laboratory testing, trends are observed conclusions are made and ultimately summarized.

4.1 Compression Testing Results

In order to obtain compressive strengths of a concrete sample, the cross sectional area is first found. Each specimen is turned on its side to prevent the troweled top surface from being in the compression plane. Although each dimension is measured three times,

only the depth and width are used for the compressive strength. The cross sectional area is then calculated from the average depth and width using Equation (4.1):

$$Cross\ Sectional\ Area = d_{ave}\ x\ w_{ave} \qquad \text{Eq. (4.1)}$$

Where:

- Cross sectional area is in units of in.^{2}
- d_{ave} = average depth (in.)
- w_{ave} = average width (in.)

Once the specimens are measured they are tested according to the methodology outlined in Chapter 3.4. After the compression testing is concluded and the peak load recorded, the compressive strength of the sample is determined from Equation (4.2):

$$f'_c = \frac{P}{A} \qquad \text{Eq. (4.2)}$$

Where:

- f'_c = Compressive strength in pounds per square inch (psi)
- P = max load obtained by sample (lbs)
- A = Cross sectional area calculated from Eq. 1 (in.^{2})

The standard deviation and coefficient of variation are also calculated for each parameter. These results are shown in Table 4.1.

Table 4.1: Average Compressive Strength

Mix Design	f'c (psi)	Standard Deviation (psi)	Coefficient of Variation
Control	20,314	2,764	13.60%
Silica Fume 1	16,190	2,308	14.20%
Silica Fume 2	15,448	3,195	20.70%
Silica Fume 3	19,770	2,343	11.90%
Silica Fume 4	14,529	3,125	21.50%
Water 1	16,550	2,151	13.00%
Water 2	18,505	2,124	11.50%
Water 3	21,073	3,093	14.70%
Sieve 1	17,200	6,715	39.00%
Sieve 2	17,145	2,758	16.10%

It can be seen in Table 4.1 that the highest compressive strength obtained is 21,073 psi from the mix design "Water 3". A common mechanical property of Portland cement concrete is that the compressive strength is inversely proportional to its water to cement (w/c) ratio. This is proven in the water replacement study where the highest compressive strength is attributed to the lowest w/c. The compressive strength consequently drops as the w/c ratio is increased. Apart from "Water 3" all compressive strengths are below that of the control mix design. All mix designs' coefficient of variation generally hold in the 10-20% range with one exception being "Sieve 1" at 39.00%. To observe any trends for each mix design, each parameter is plotted along with

the control and is presented in the following sections. A complete record of all the raw data for compression testing can be found in Appendix C.

4.1.1 Compressive Strength: Silica Fume Replacement

The silica fume in Ultra High Performance Concrete (UHPC) has multiple functions in the performance of the concrete. It acts to fill in the micro-voids of the cement matrix, enhances the rheology, and produces a secondary hydration through a pozzolonic reaction (Allenaet. Al, 2011). Due to the various roles that silica fume plays, it is necessary to see if there is an optimum percentage of the silica fume replacement. For this parameter, the silica fume percent replacement is both increased and decreased by 10% and 20% from the control.

In terms of silica fume replacement, no general trends are observed in the compressive strength as shown in Figure 4.1. However, the control has the highest compressive strength and “Silica Fume 3” has a slightly lower compressive strength. The other three mix designs have significantly lower compressive strengths. Due to the multiple functions of silica fume, it is difficult to conclude as to why the compressive strength decreased with the three different mix designs. It is also difficult to ascertain why the strength drops from “Silica Fume 1” to “Silica Fume 2” then rises back up to the “Control” mix. However, once the compressive strength and energy absorption are considered together, the mechanical contribution of silica fume to UHPC becomes more evident. This discussion is presented later in this chapter.

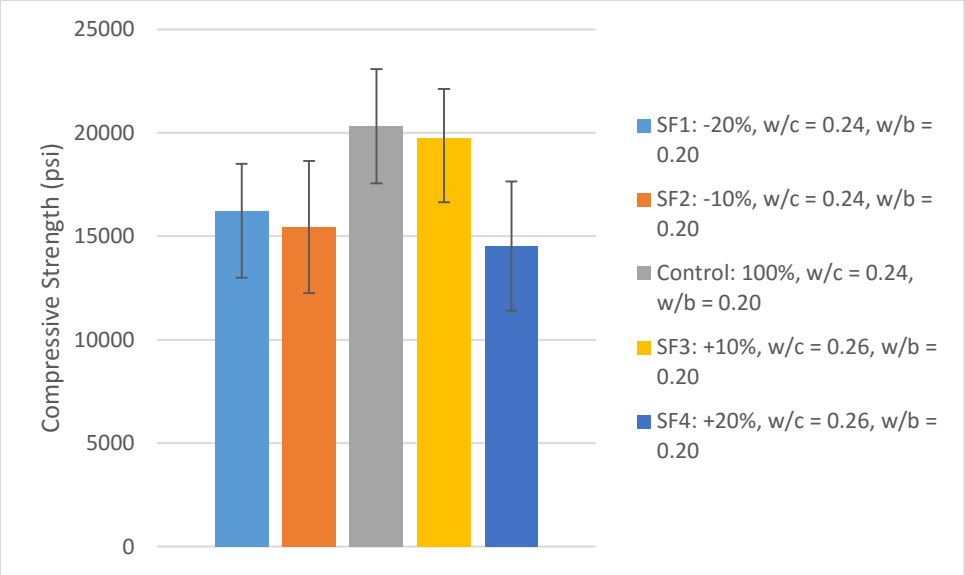

Figure 4.1: Silica Fume Replacement: Average Compressive Strengths

4.1.2 Compressive Strength: Water Replacement

Due to the fact that UHPC already has a very low w/c and water to binder (w/b) ratio, this ratio is only increased and decreased by 2.5% and 5%. During testing, a mix with a w/b ratio of 0.16 is attempted. The mix is determined to be too dry to cast quality specimens and therefore discarded. The remaining mixes however are cast and tested. Figure 4.2 illustrates the trend in compressive strength when the water to binder ratio is altered. As the w/b ratio decreases, the compressive strength increases. As stated previously, this holds true with the common mechanical properties of Portland cement concrete. It can be seen from Figure 4.2 that the compressive strengths also follow an approximate linear trend in the increase of compressive strengths.

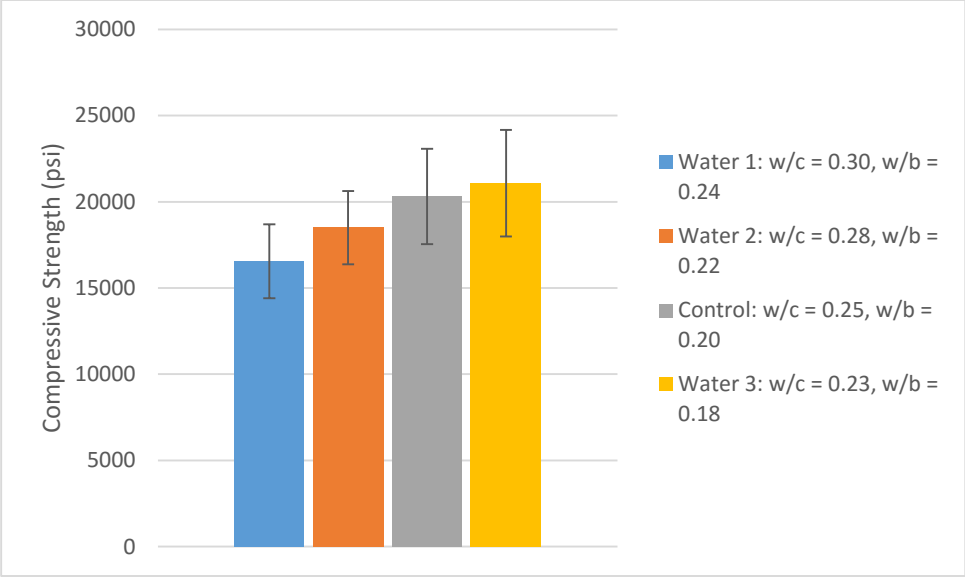

Figure 4.2: Water Replacement: Average Compressive Strength

With a compressive strength of approximately 21 ksi, mix "Water 3" is found to have the highest compressive strength. This is not only the most for the water replacement, but of all mix designs tested in this thesis. Although it may have the highest compressive strength it also has the highest standard deviation. This higher standard deviation can be attributed to the lack of water. It is observed in the casting of the specimens that this batch is much less workable than the other ones; therefore, a decline in the homogeneity of the samples exists. From these results it becomes apparently clear that the compressive strength is very sensitive on the mix's water to cement/binder ratio. A small change in water can result in a significant change in compressive strength.

4.1.3 Compressive Strength: Sieve Replacement

The quartz sand used in this study is a commercially available quartz sand. As stated in Chapter 3.1, the sand is sieved through a #30 sieve. The sand is initially attempted to be sieved through a #10 and #40 sieve (one size larger and smaller than a #30), but the sand either completely passes through the #10 or is entirely retained on the

#40 sieve. Due to the particle size being extremely binary of either passing or retaining on the #30, the mix designs presented for gradation are consequently used. In order to further study the effects of gradation on the mix design, a better graded quartz sand product would need to be used.

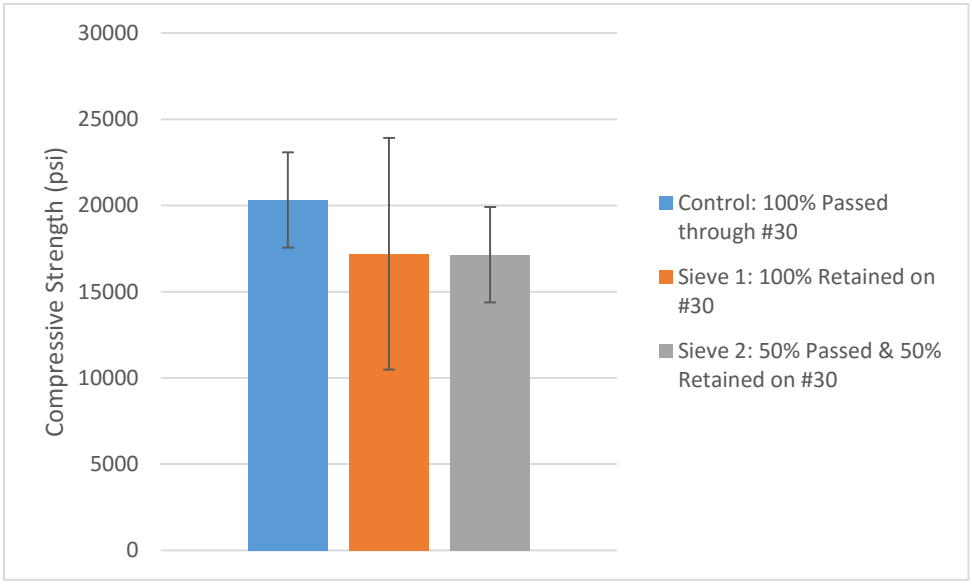

Figure 4.3: Sieve Replacement: Avg. Compressive Strength

Figure 4.3 shows that there is one trend when it comes to the gradation effects on compressive strength. The observed trend is when there are sand particles larger than the #30 sieve in the cement matrix, the compressive strength decreasess. From this testing, the compressive strengths are nearly identical for both mix designs “Sieve 1” and “Sieve 2”. One of the goals of UHPC is to ensure a densely compacted uniform mix. The fine quartz sand fills in the voids of the cement matrix allowing for this to happen. When larger particle sizes are added, the homogeneity of the mix is compromised and ultimately affects the compressive strength. The mix design that has 100% of the quartz sand retained on the #30 sieve also has the largest standard deviation. This is also attributed to the inconsistency of the cement matrix from the larger particle sizes.

The compressive strengths for all three parameters in conjunction with the energy absorption results are used to make the conclusions relevant to the objectives of this thesis and can be found in Section 4.3. A full breakdown for every sample tested in compression including average dimensions and ultimate strength can be found in the Appendix C.

4.2 Energy Absorption Rates

As is with the compressive samples, each Charpy testing specimen is measured three times on each of its dimensions. In order to determine the energy absorbed only one dimension is used; the width across which the pendulum acts. The energy absorption is calculated according to Equation (4.3):

$$\tau = \frac{U}{h} \qquad \text{Eq. (4.3)}$$

Where:

- τ = Shear Strength (ft-lb/in)
- U = Energy Absorbed (ft-lb)
- h = Thickness of the sample (in)

The dimension “h” used in the previous calculation is the distance across the sample through which the pendulum travels. This is used to normalize the strengths across the given specimen. This dimension is illustrated in Figure 4.4.

Figure 4.4: Charpy Specimen Dimension

At the conclusion of testing, all results are plotted for each parameter. These plots can be seen in Figures 4.5-4.7. For each parameter it becomes obvious that major outliers in the testing exist. These outliers are indicated in the plots by triangles as opposed to dots. These values are removed from the results of the testing so that the trends from testing can be readily determined. It should be noted, that none of the mixes have more than one outlier removed.

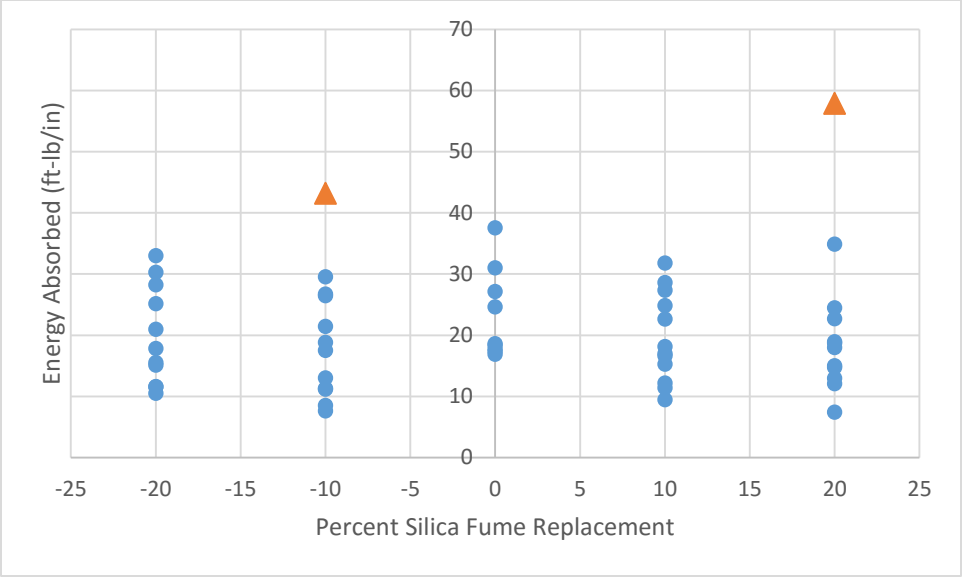

Figure 4.5: Energy Absorbed: Silica Fume Replacement

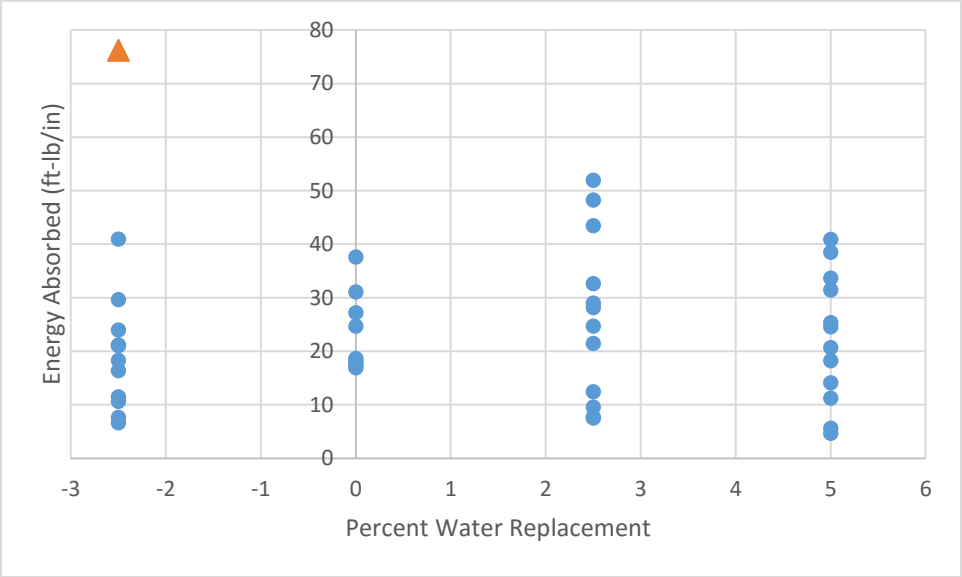

Figure 4.6: Energy Absorbed: Water Replacement

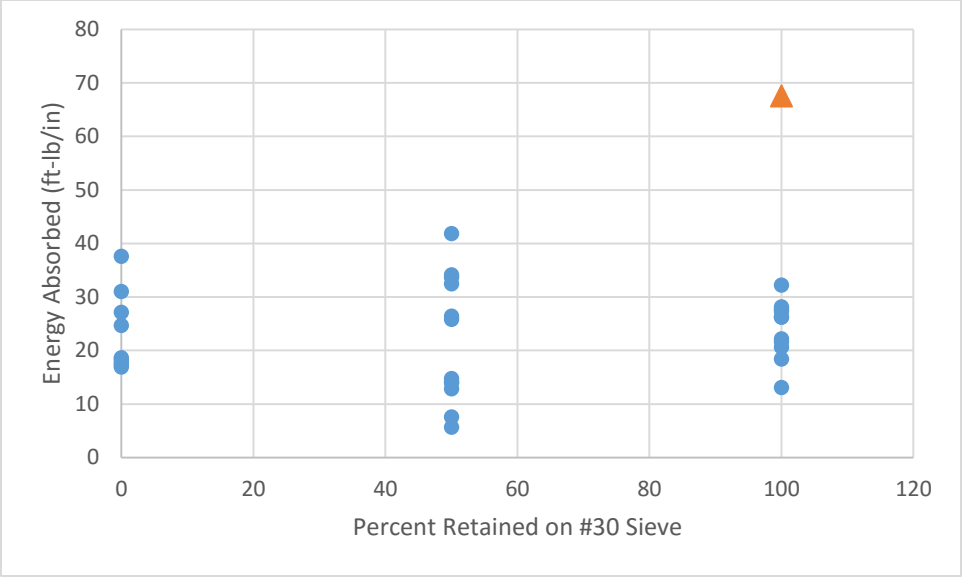

Figure 4.7: Energy Absorbed: Sieve Replacement

Once the outliers are discarded, the data is analyzed. From the collected data, the average value, standard deviation, and coefficient of variation are calculated. These values are presented Table 4.2.

Table 4.2: Average Energy Absorption

Mix Design	**τ (ft-lb/in)**	**Standard Deviation (ft-lb/in)**	**Coefficient of Variation**
Control	23.3	7.37	31.20%
Silica Fume 1	20	8.06	40.30%
Silica Fume 2	17.5	7.76	44.40%
Silica Fume 3	19.6	7.3	37.30%
Silica Fume 4	18.2	7.4	40.40%
Water 1	22.4	12.2	54.40%
Water 2	26.4	15.6	59.10%
Water 3	18.9	10.2	54.10%
Sieve 1	24	5.4	22.50%
Sieve 2	22	11.9	54.30%

The results from Table 4.2 show that the largest impact energy absorption comes from “Water 2” with an average value of 26.4 ft-lb/in. The lowest values come from “Silica Fume” with an average value of 18.2 ft-lb/in. The other result that is very apparent from this table is the large values of coefficient of variation obtained through the testing. These values range anywhere from 22.5%-59.1%, which is significantly higher than the values obtained in the compressive strength testing. However, this is partially to be expected as the Charpy test is a relative test and has more potential for error. A full breakdown of all Charpy testing data for each specimen can be found in Appendix D.

4.2.1 Energy Absorption: Silica Fume Replacement

As is with the case of the silica fume for compressive strength, no general trends are observed with the energy absorption. The control exhibits the highest energy absorption as with the compressive strength. Due to the multiple uses of silica fume, even slight changes in the concentration gives varying differences in the energy absorption. This makes the analysis of the behavior of the cement matrix difficult to understand as well as to track the trends that may be occurring.

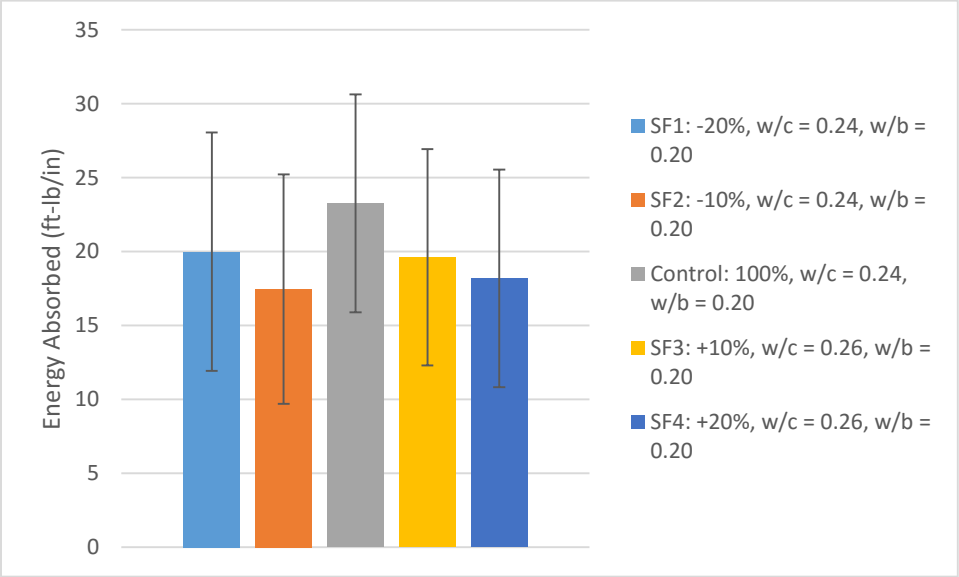

Figure 4.8: Silica Fume Replacement: Average Energy Absorbed

From Figure 4.8, the highest enegy absorption rate belongs to control with a value of 23.3 ft-lb/in and a coefficient of variation of 31.20%. The lowest value is “Silica Fume 2” with an average value of 17.5 ft-lb/in of energy with a coefficient of variation of 44.4%. This also happens to be the highest coefficient of variation for any of the mixes in the silica fume parametric study. The coefficient of variations for this parametric range from 31.2%-44.4%.

It can be noted however, (and as shown in Figure 4.8) that the trend observed in the compressive strength follows the same trend that is seen in the energy absorption. The energy absorption drops from “Silica Fume 1” to “Silica Fume 2” then peaks at the “Control” mix design. From there the energy absorption drops again from “Control” to “Silica Fume 3” and continues declining to “Silica Fume 4.” This similar behavior confirms the trends observed for the strengths in the silica fume replacement study. Due to the similar trends observed in both the compressive strength and energy absorption, it can be concluded that the shear failures associated in impact loads are not attributed to the silica fume concentration.

4.2.2 Energy Absorption: Water Replacement

The results from the Charpy testing on the water replacement specimens is shown in Figure 4.9. The mix design with the highest energy absorptions is “Water 2”. The average energy absorbed for this mix is 26.4 ft-lb/in. The control is similar to “Water 1” with average values of 23.3 ft-lb/in and 22.4 ft-lb/in respectively. Although “Water 2” has the highest average energy absorption, it also boasts the highest coefficient of variation for the given parameter. “Water 3” has the lowest energy absorption at a rate of 18.9 ft-lb/in.

Unlike the silica fume parametric study results, the energy absorption rates do not follow the same trend as the compressive strength for water replacement. The compressive strength followed a linear progression where the compressive strength increased as the w/b ratio decreased. For the energy absorption, the rate peaks at “Water 2” and decreases from there. It can be concluded that the water content has an effect on the energy absorption rates and shear failure for UHPC under impact loading.

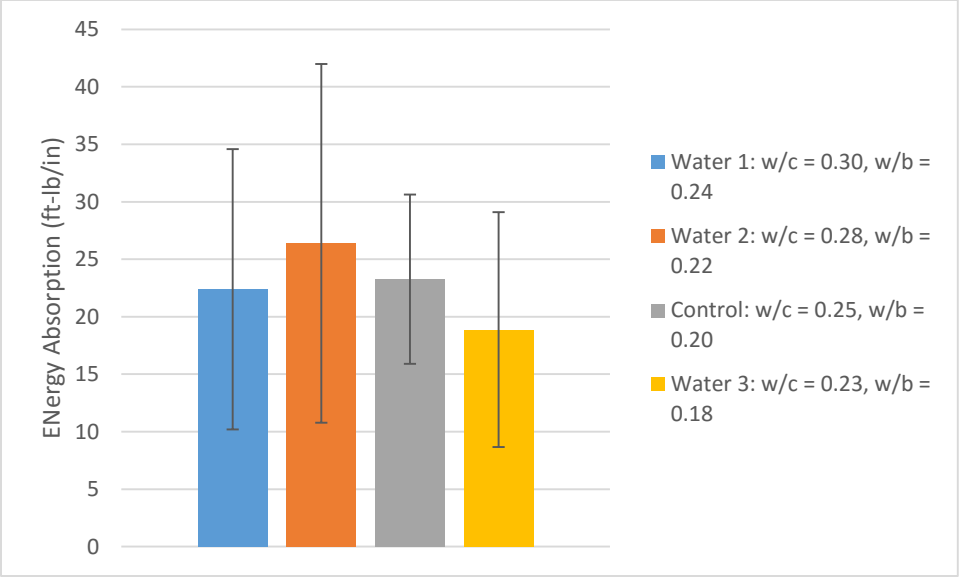

Figure 4.9: Water Replacement: Average Energy Absorbed

4.2.3 Energy Absorption: Sieve Replacement

In the case of the sieve replacement parameter for energy absorption, "Sieve 1" has highest average energy absorption with 24.0 ft-lbs/in. This mix design contains quartz particles only retained on the #30 sieve. The energy applied to the specimen must not only fail the cement matrix, but also the fine grain particles. The larger particles require more energy to fracture and therefore they facilitate a larger energy absorption. "Sieve 1" is only slightly higher than that of "Control" with an average value of 23.2 ft-lb/in. "Sieve 2" drops off slightly and has an average energy absorption of 22.0 ft-lb/in.

Between the control and two sieve mixes, "Sieve 2" has the highest coefficient of variation. For similar reasons attributed to the lower value in compression, those larger particles once again compromise the homogeneity of the concrete matrix. Although "Sieve 1" also has the larger quartz particles, the cement matrix is homogenous where "Sieve 2" has a mix of large and small particles. Due to this mix of grain sizes, the

cement matrix is not uniform throughout, causing a larger coefficient of variation. These trends can be seen in Figure 4.10.

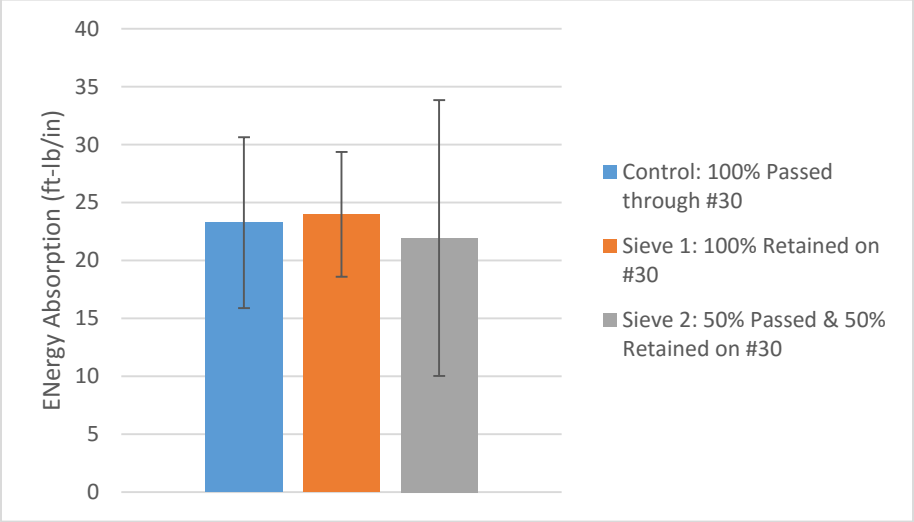

Figure 4.10: Sieve Replacement: Average Energy Absorbed

4.3 Compressive Strength vs Energy Absorption Correlation

The main objective of this thesis is to study any trends that are associated between the compressive strength of concrete and the energy absorption for the given parameter. In order to accomplish this, a ratio is established between the compressive strength and the energy absorption. This ratio is then plotted against the parameter associated with the mix design and the resulting trends are observed.

As is the case for most things in this world, the use of concrete design is driven by money. A general trend for concrete states that "As the compressive strength increases, it becomes increasingly expensive." Taken into account this relationship, one can question if there is a way to increase the energy absorption at a lower cost and consequently a lower compressive strength. In relation to blast and impact loading this is an acceptable tradeoff because the design properties associated with compressive strength can be improved using reinforcing steel. With compressive strengths of UHPC being so high,

they may be sacrificed, if needed, to gain energy absorption as well as to reduce the cost. In following this approach, the cost ratio for energy absorption can be derived from Equation (4.4):

$$\$/_{ksi} * ksi \div e.a. = \$/_{e.a.} \qquad \text{Eq. (4.4)}$$

Where:

- $/ksi = the unit cost of concrete per compressive strength
- ksi = the given compressive strength for the mix
- e.a. = the associated energy absorption for the mix

In using this equation and taking the ratio of the compressive strength to the energy absorption, the ratios can then be calculated and plotted. The resulting values however are relative values and not an actual cost analysis. The use of this equation and associated plots provides the analysis needed to identify mix designs that may sacrifice compressive strength but in turn gain strength in energy absorption. The process of following this method allows one to identify more efficient and generally cheaper methods to develop a stronger mix design for energy absorption. Therefore, in using these plots, a lower values indicate a lower cost per unit of energy absorption which is therefore considered more desirable. Trends can then be observed on this relationship between the compressive strength and energy absorption for each parameter.

4.3.1 Compressive Strength vs. Energy Absorption Correlation: Silica Fume Replacement

The results shown in Figure 4.11 are obtained using composed the method developed in the previous section. The y-axis is the average compressive strength divided by the average energy absorption values. The x-axis is the percent replacement of silica

fume in the mix. At the top of the plot on the x-axis, the mix design's designated names can be seen. Using this plot, the trends of the effect of compressive strength on the energy absorption can be seen.

From Figure 4.11 it is observed that "Silica Fume 4" has the lowest ratio of compressive strength to energy absorption. This is due mainly in part to the relatively low compressive strength that "Silica Fume 4" possesses. With a compressive strength of only 14.5 ksi and then a energy absorption rate of 18.2 ft-lb/in, the ratio results in a value of 0.797. The next lowest value is that of "Silica Fume 1." This mix had a slightly higher compressive strength of 16.2 ksi, but the energy absorption rate increased as well to 20.0 ft-lb/in giving a ratio value of 0.81.

Although the "Control" has the highest compressive strength of the silica fume, it also has the highest energy absorption rate at 20.3 ksi and 23.3 ft-lb/in respectively. This total ratio value of 0.871 lands "Control" as the 3rd lowest ratio mix design in the silica fume replacement study. Following closely behind "Control" is "Silica Fume 2" with a ratio of 0.88 resulting from an average compressive strength of 16.2 ksi and energy absorption of 20.0 ft-lb/in. The greatest ratio is found to be "Silica Fume 3." Of all the mix designs in silica fume replacement study, this is the only mix to have a ratio greater than 1. With an average compressive strength of 19.8 ksi and average energy absorption rate of 19.6 ft-lb/in, the resulting ratio is 1.01. The general trend that silica fume follows is that the efficiency decreases as the silica fume increases. Mix design "Silica Fume 4" however does not follow this trend, thus showing that there is an optimum value of silica fume inclusion and after this point, the efficiency of including silica fume in the mix decreases.

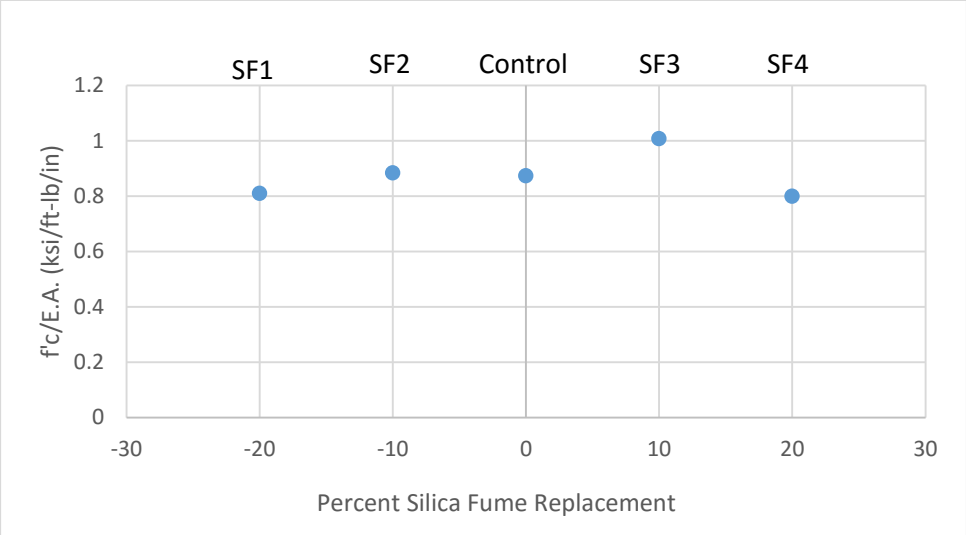

Figure 4.11: f'c vs. E.A.: Silica Fume Replacement

4.3.2 Compressive Strength vs. Energy Absorption Correlation: Water Replacement

The same procedures as stated previously are followed to observe the correlation of compressive strength and energy absorption for the water replacement parameter. Using the plot presented in Figure 4.12, trends can be observed in the correlation for the water replacement study.

In the observation of Figure 4.12, it is determined that the lowest efficiency value is attributed to mix design "Water 2." This value is not only the lowest for the water replacement study, but also the lowest for the entire parametric study of this thesis. The average compressive strength of "Water 2" is 18.5 ksi with an energy absorption rate of 26.4 ft-lb/in. This energy absorption rate corresponds to the highest rate for any mix design in this thesis which contributes to the lowest ratio value of 0.70.

The next lowest ratio belongs to "Water 1." This mix design has the lowest compressive strength for all water replacement mixes of 16.5 ksi, but it has a relatively higher energy absorption rate of 22.4 ft-lb/in. This results in a ratio of 0.74 for "Water 1."

The control has the next lowest ratio of 0.871 for the same values as stated in silica fume replacement.

Although “Water 3” may have had the highest compressive strength of 21.1 ksi, it has a relatively lower energy absorption rate of 18.9 ft-lb/in resulting in the highest ratio for this thesis study with a value 1.12. The overall trend for water replacement is that as water content is decreased, the efficiency of the mix decreases as well.

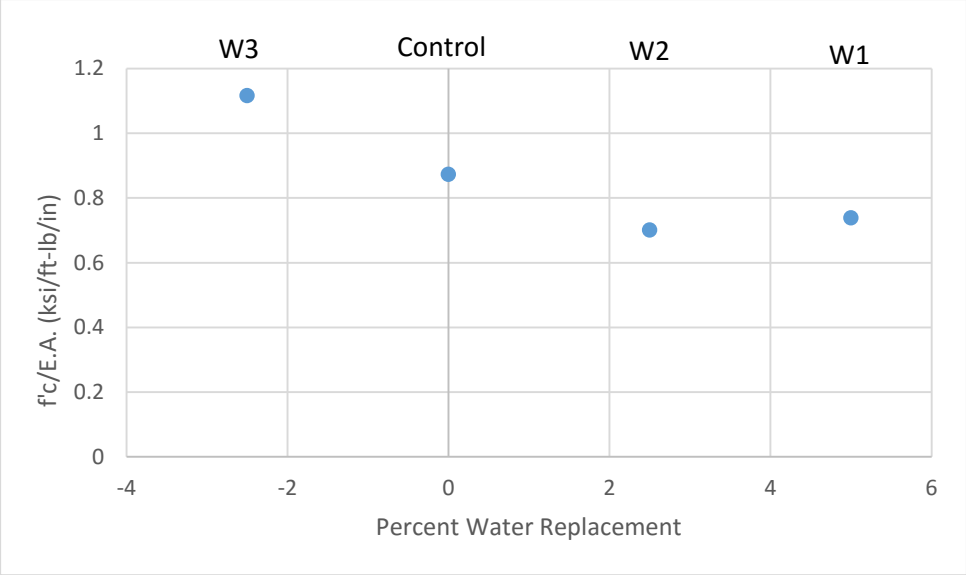

Figure 4.12: f'c vs. E.A.: Water Replacement

4.3.3. Compressive Strength vs. Energy Absorption Correlation: Sieve Replacement

As is the case with the previous two parameters, the plot is once again assembled in similar fashion. The y-axis is the same with the x-axis displaying the percent retained on the #30 sieve and the accompanying mix design designation on top. From the plot in Figure 4.13, the trends are observed for the sieve replacement.

It is observed in Figure 4.13 that “Sieve 1” has the lowest ratio of 0.716. Although its compressive strength is significantly lower than the “Control” with a value of 17.2 ksi,

it has an exceptional energy absorption rate of 24.0 ft-lb/in. This disparity between the energy absorption and compressive strength provides for such a low ratio. “Sieve 2” also has similar mechanical properties with a compressive strength of 17.1 ksi and energy absorption of 22.0 ft-lb/in. Although the energy absorption rate is only slightly lower than that of “Control”, the lower compressive gives a lower ratio of 0.78. This is lower than the “Control” ratio value of 0.871. This shows that although the larger quartz sand particles may be detrimental in the compressive strength, the energy absorption rates benefit from the inclusion of these particles in the mix.

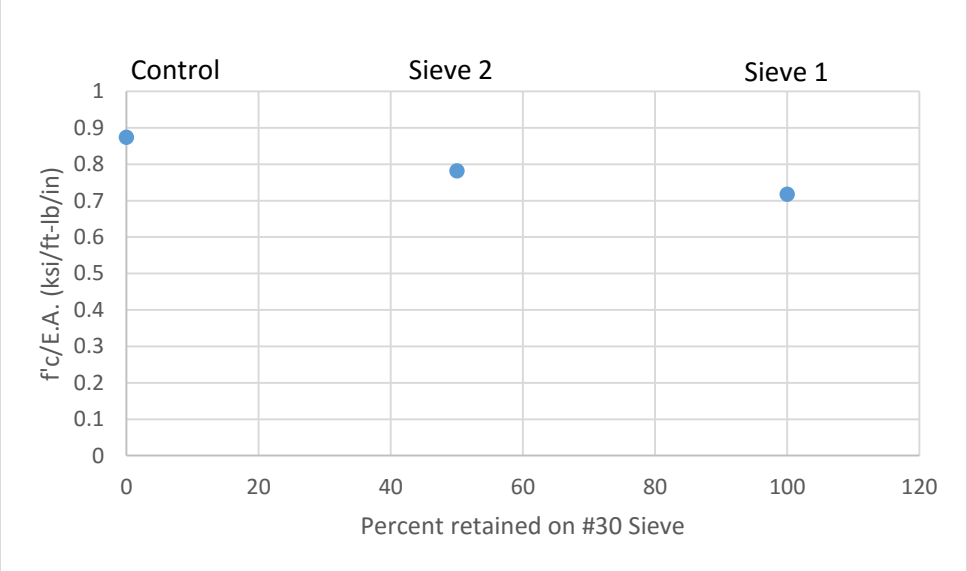

Figure 4.13: f'c vs. E.A.: Sieve Replacement

4.4 Optimum Mix Design

The final objective of this thesis is to determine an optimum mix design. In the previous section the mix design is selected based on an efficiency. Where can compressive strength be sacrificed to gain energy absorption? In this analysis however an optimum mix design is selected based on overall strength. Which mix design has the

most strength when it comes to both compressive strength and energy absorption? To determine the optimum mix design, Equation 5.1 is used.

$$Q = \frac{E.A.x\sqrt{f'c}}{max|E.A.x\sqrt{f'c}|} \quad \text{Eq. (5.1)}$$

- Q = Mix Design Ratio (unitless)
- E.A. = Energy Absorption (ft-lb/in)
- f'c = Compressive Strength (ksi)
- max = maximum value for each parameter studied (ft-lb/in * ksi)

This method signifies a normalized value for the optimum mix design. It takes into account both the compressive strength and energy absorption to suggest which mix has the greatest strengths for both parameters. The shear strength of concrete is typically a function of the square root value of the compressive strength; therefore, since the energy absorption is attributed to the shear strength, the square root of the compressive strength is taken. In dividing these ratios by the maximum value for each parameter, the most optimum mix design is represented by a value of one. Subsequent optimizations are then signified by the decimal numbers. These optimum mix designs are shown in Figures 4.14-4.16.

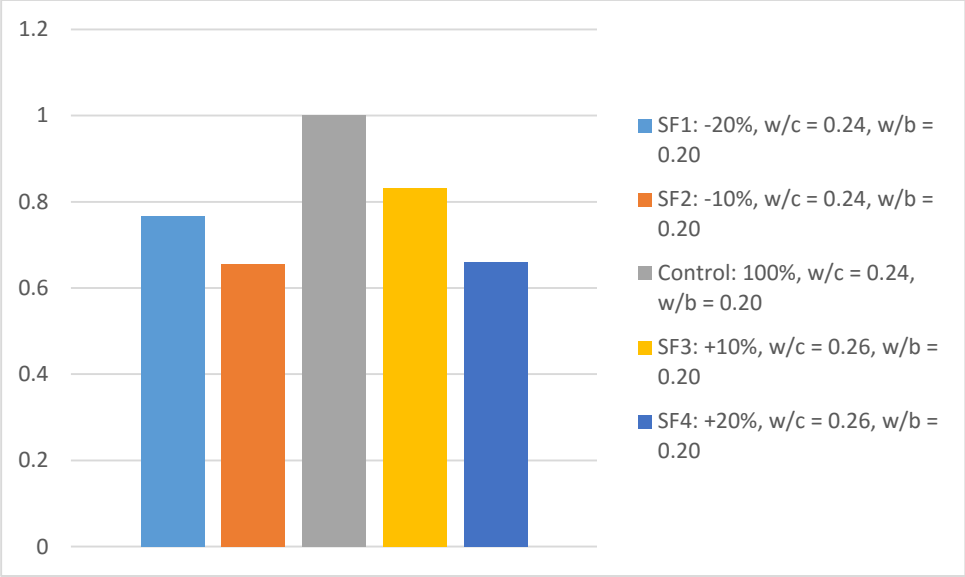

Figure 4.14: Silica Fume Replacement: Optimum Strength

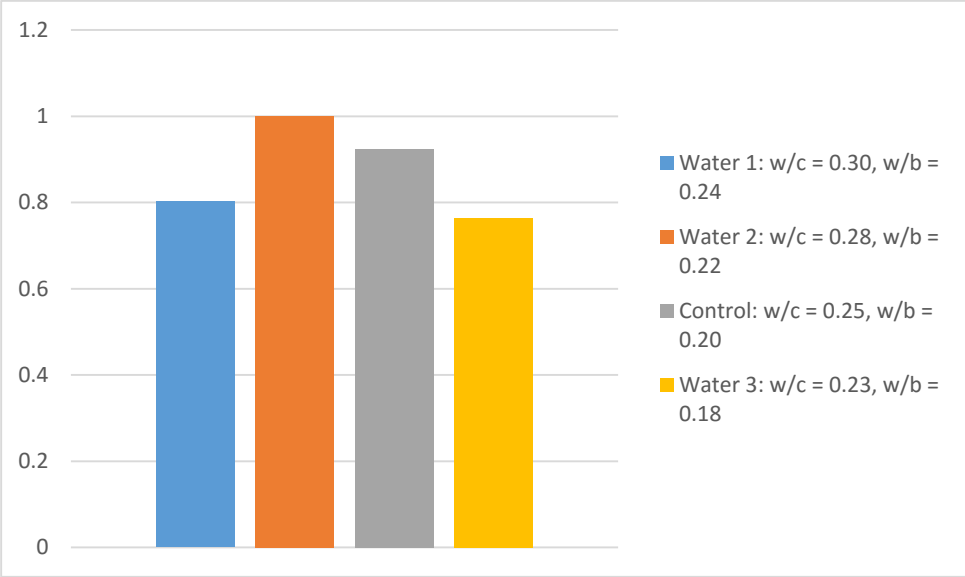

Figure 4.15: Water Replacement: Optimum Strength

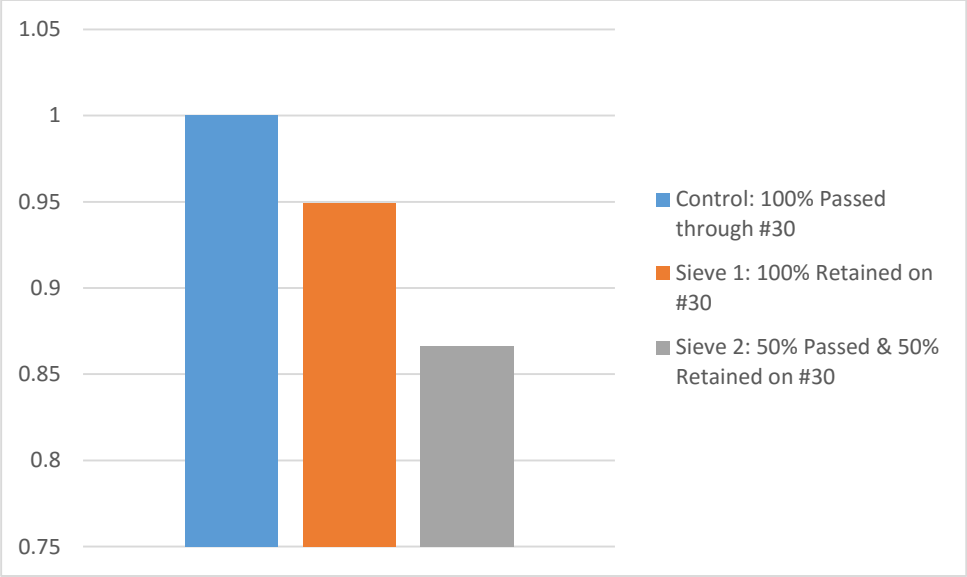

Figure 4.16: Sieve Replacement: Optimum Strength

It can be seen in Figure 4.14 that “Control” is the optimal mix for the silica fume replacement. Due to “Control” having the highest compressive strength and energy absorption for the silica fume parameter, it is easy to see why this is the optimum mix. The trend observed for the silica fume also follows the same trend seen for both the compressive strength and energy absorption. For this trend, “Water 2” is shown to be the optimum mix. Although the compressive strength is lower for this design, the higher energy absorption made it the more optimum mix. This general trend observed also follows the same one for water replacement and energy absorption and is shown in Figure 4.15. For sieve replacement, “Control” is once again deemed the optimum mix. Although it has a lower energy absorption than “Sieve 1” the much higher compressive strength proves it to be a more optimized mix as shown in Figure 4.16.

From the optimization analysis, an optimum mix design can be selected. To do this, all the mix design values from each parameter are compared before they’re normalized. The mix that presents the highest optimization is “Water 2” with a value of

113.5. The next highest value is “Control” with a value of 104.8 and the remaining mixes all have values below 100.

4.5 Conclusions

From the analyzed data, some overall conclusions can be made about the mix constituents and their effects on the compressive strength and energy absorption rates of UHPC. These conclusions outline the general trends that are observed in UHPC in terms of compressive strength, energy absorption, and the correlation between them. In examining these trends, the behavior of UHPC becomes better understood under certain loading conditions.

4.4.1 Conclusions: Compressive Strength

The increase in sample size proved relatively effective in obtaining accurate data for the compressive strength of the UHPC. The coefficient of variation ranged from 11.5% to 21.5% with one exception being 39.0%. Although a statistical value for UHPC is not provided by Nowak and Collings (2013), typical values range from 11.0% to 15.5% for normal weight and high performance concrete. Although the coefficient of variations for this study reside slightly higher than those values listed, they are with an acceptable proximity. A further increase in sample size could assist in closer target values.

For the average values of compressive strength, both predicted and unforeseen trends are observed. The trends of silica fume show that there is an optimal content of silica fume to gain an optimum compressive strength. Decreasing the silica fume presents an immediate drop in compressive strength; however, continual decrease shows an

increase in the compressive strength. Increasing the content of silica fume from the optimum shows a gradual decrease in the compressive strength. Due to the multi-purpose function of silica fume, this trend is not necessarily unexpected.

The average compressive strength trends that are observed in water replacement are as expected. These trends follow basic Portland cement concrete behavior for compressive strength; as the water content decreases, the compressive strength increases. Not only do the compressive strengths increase, they follow a very linear trend. It is found however that there becomes a point that there is not enough water. If that water content drops too low, then proper concrete specimens cannot be cast and therefore the sample is unusable. These trends are as expected for the compressive strength of concrete.

A major component in developing UHPC is to ensure a homogenous and dense cement matrix. The compressive strength testing of UHPC during the sieve replacement testing helps to confirm this theory. It is observed when larger quartz particles are introduced to the mix, the compressive strength deteriorates because of it. These larger particles compromise the homogeneity of the mix and the compressive strength suffers as a result.

4.4.2 Conclusions: Energy Absorption

Due to the lack of research in energy absorption of concrete, average statistical parameters are not known. The coefficient of variations in this study range from 22.5% to 59.1%. Although these values are relatively high for structural materials, the trends observed follow those that are expected; therefore, the values are accepted and analyzed.

When it comes to the energy absorption for silica fume replacement, the trend observed follows the same trend as the compressive strength for the same reasoning of the multi-functionality of the silica fume. Although still unknown exactly why this trend is followed, the similarities between the compressive strength and energy absorption support this theory. Due to the energy absorption following the same trends as compressive strength, is can also be concluded that the silica fume is not a contributing factor to shear failures under impact loading.

In the study of water replacement's effect on energy absorption, the trend does not follow that of the compressive strength. The average energy absorption reaches a peak at a given water content and declines as the water content is either increased or decreased. This peak happens to be at a water content greater than that of the control mix. The increased water allows for greater workability and therefore an increase in the quality of the cement matrix. This increase in quality provides for a greater energy absorption under the impact loads. The cement is very sensitive to changes in water. These trends show that the water content of the mix design contribute to the shear failure behavior under impact loading.

For the sieve replacement study, the trends of the energy absorption does not follow that of the compressive strength. The addition of larger particles proved to decrease the compressive strength of the mix. In the case of energy absorption, the larger particles increased the strength of the mix. The impact load is not only required to break the cement matrix, but the aggregates as well. These larger quartz sand particle provide for more energy absorption as the load is applied to the concrete. An overall conclusion

can be made that the quartz sand particle size can directly contribute to shear failures under impact loads.

4.4.3 Conclusion: Compressive Strength vs. Energy Absorption

The main objective of this thesis is to determine any correlations between the compressive strength and energy absorption for the UHPC. In doing this, it is possible to see if there are any ways to sacrifice compressive strength in order to gain energy absorption. In doing this, a more economical mix design can be used to obtain higher energy absorption rates. Reinforcing steel can always be added to a structure to increase its flexural strength; however, the energy absorption is mostly reliant on the concrete.

The general trend for silica fume shows that as the silica fume is increased, the efficiency of the mix decreases. Although a lack of silica fume compromises the compressive strength of the UHPC, the energy absorption rates are relatively unscathed. In using this trend, a mix design that utilizes a lower silica fume produces a more effective UHPC in terms of energy absorption. In the study of water replacement the trend is evident; as the water content increases, the mix design becomes more efficient. Although lowering the water content allows for higher compressive strengths, this does not lead to an increase in energy absorption. This value however does reach a peak efficiency when the water content reaches a certain point. Knowing this, additional water can be added to a mix to increase the energy absorption at a sacrifice to compressive strength.

For the correlation of compressive strength to energy absorption in the sieve replacement study, it is found that the efficiency of the mix is inversely proportional to that of the compressive strength. Although the smaller quartz particles allow for a

stronger compressive strength, there isn't a large gain in the energy absorption as a result of it. The addition of only large particles provides for the same compressive strength as a blend of both large and small particles. However, a mix that relies solely on large particles provides the most efficient mix for energy absorption.

4.4.4 Optimum Mix Design

The optimum mix design is calculated by the product of the square root of the compressive strength and the energy absorption rate and then normalized. In using this process, it is found that "Control" is the optimum mix design for the silica fume and sand gradation parameters. However in the water parameter, it is found that "Water 2" is the most optimum mix design. "Water 2" also happens to be the most optimum mix design of all mixes tested in this research due to its relatively high compressive strength and its exceptionally high energy absorption.

CHAPTER 5

SUMMARY, CONCLUSION, and FUTURE WORK

5.1 Summary and Conclusions

5.1.1. Methodology Summary

To accomplish the objectives of this research project, laboratory testing of Ultrah High Performance Concrete (UHPC) specimens in undertaken. To provide for accurate results, relevant ASTM standards are followed when possible. In instances where no standards are applicable, adjustments to related ASTM standards using best engineering judgement is practiced. There are also cases where the ASTM standard cannot be followed precisely; in such cases, adjustments are made to conform to the standard as closely as possible.

The testing of UHPC introduces intricacies that are not typically encountered in the testing of normal strength concrete. The higher strengths exhibited by UHPC not only present for issues in end condition preparation of compression testing, but also the capacities of the testing machinery are approached. Therefore the first objective of this thesis is to develop accurate testing methods for UHPC specimens. In order to do this, ASTM C109 is followed. Adhering to this standard addresses both issues stated previously. The end conditions are accounted for and smaller samples do not extend the loading limits of the testing machinery.

In conjunction with Objective 1 (as stated in Chapter 1), the second objective is to establish mixing and curing methods that provide for a control mix design using local

materials. A mix design presented by Allena and Newtson (2010) is selected for the control. Conventional concrete mixing and curing practices are used as a guideline. However, due to the nature of UHPC these guidelines require adjustment. This biggest adjustment is the mix time required for UHPC which can take anywhere from 30-90 minutes to mix. The UHPC specimens are cured in a lime water bath as standard suggests. However they are cured at higher temperatures and ultimately oven cured during the final two days of curing to enhance the pozzolonic reaction. In following this methodology Objective 2 is met.

The use of local materials allows parameters to be identified and consequently modified to study their effects. To complete Objective 3, the constituent parameters studied are the silica fume replacement, w/c ratio, and fine sand gradation. To study their effects each parameter is altered from the control. For the silica fume, the percent replacement is either increased or decreased by 10% and 20%. The w/c ratio is increased and decreased from the control by 2.5% and 5%. And lastly the gradation of the sand has one mix with all sand particles retained on the #30 sieve and the second has a blend with half the particles retained on the #30 sieve and the other half that passes the #30 sieve.

Once the mixing, curing, and compression testing methods are met, the development of a test method that models impact/blast loads on UHPC ensues. It is determined that this loading can be modeled utilizing Charpy impact testing methods. Although ASTM E23 is the standard for Charpy impact of metallic specimens, no current standards for concrete specimens exist. Therefore ASTM E23 is followed as closely as possible. In using this testing, impact and blast loads can be subjected to the concrete specimens and their results obtained fulfilling Objective 4.

5.1.2. Results Summary

After all the testing is completed for both compression and Charpy impact testing, the results are obtained and analyzed. Each parameter is investigated for both testing setups, trends are observed, and the results compared. From these results, a correlation between both testing methods is developed to complete Objective 5. This correlation illustrates what is the best efficiency for each mix design. The efficiencies demonstrate mix designs that have the capability to sacrifice compressive strength to obtain higher energy absorptions for impact and blast loads.

The compression testing values range from 14.5 ksi to 21.0 ksi with the control having a compressive strength of 20.3 ksi. Coefficient of variation values range from 11.5% to 39.0%. The trends in silica fume are as a result of the multi-functionality of silica fume in the cement matrix. The water to cement ratio follows the basic mechanical principles for compressive strengths of concrete. And lastly the trends observed in sand gradation show that once larger sand particles are introduced to the cement matrix, the compressive strengths deteriorate.

The Charpy impact testing values range from 17.5 ft-lb/in to 26.4 ft-lb/in with the control exhibiting a strength of 23.3 ft-lb/in. The coefficients of variation for this testing are much higher than the compression strengths with a range of 22.5% to 59.1%. The trends observed in the silica fume follow the same trends as the compressive strength. This not only confirms the behavior of the addition of silica fume, but also infers that silica fume does not contribute to the shear failures associated with impact loads. The water to cement ratio does not follow the same trends as the compressive strength and sample preparation is one of the causes for this. It is observed that larger sand particles

allow for higher energy absorptions even though the compressive strengths suffer as a result.

In order to determine an efficiency of the mix designs and note any correlations between compressive strength and energy absorption, a ratio of these two strength parameters are calculated and plotted. It is observed for silica fume that the efficiency generally decreases for the mix as the silica fume content is increased. The mix design efficiency increases however as the water content is increased. The same trend is observed with the sand gradation where the efficiency is increased as there is an increase in larger content of sand particles.

At the conclusion of these analysis, each parametric is ranked in order of the most influential on shear failures of concrete under impact loads to least critical. The trends observed for both compressive strength and energy absorption assist in determining the criticality of each parameter. The parameter considered to be the most critical to shear failures is the sand gradation. Although smaller grain sizes increase the compressive strength, the energy absorption drops and therefore attributes to shear failures. The next most critical parameter is the water to cement ratio. While a decrease in water to cement ratio may increase the compressive strength, an increase in energy absorption is not the case. A higher water to cement ratio can increase the energy absorption. The least critical parameter is the silica fume replacement. The similar trends for both the compressive strength and energy absorption indicate that the silica fume content doesn't have a noticeable influence on the shear strengths of UHPC.

The final objective of this research is to determine an optimum mix design. In Objective 5 a ratio of the compressive strength to energy absorption is plotted to

determine the efficiency. For the optimum mix design a different approach is taken. The product of the square root of the compressive strength and the energy absorption is calculated then each value is normalized. Although “Control” is found to be the optimum mix design for each the silica fume replacement parameter and sand gradation parameter, “Water 2” is found to be the most optimum mix. The high energy absorption and relatively high compressive strength proved to make this the most optimum mix of the study.

5.2 Future Work

As research continues to explore UHPC under impact and blast loads, there are some recommendations to not only improve this study, but also extend the research and the next steps to be taken. The obvious high variability in this thesis is the high coefficients of variation for the energy absorption. This is the first thing that needs to be addressed to not only improve the study, but also advance it as well. Once the energy absorption rates have been refined, additional parameters can be studied and their effect on energy absorption. In the end full scale modeling of impact and blast loads on concrete structures is ideal.

The lack of an ASTM Standard for the sample preparation of the concrete Charpy impact specimens proves to be an issue in this study. Although best engineering judgement is used, high coefficients of variation are a result of the lack of standard. To better standardize the specimen preparation, there are a few suggestions to improve the quality of the specimens. An improvement in specimen quality will directly increase the quality of the test results.

The first suggestion to increase the quality specimen is the use of a Harvard Miniature Compactor. Although this compactor is primarily used in soil mechanics, its use could be utilized for the compaction of the Charpy samples. The device governs the applied load every time the specimen is rodded. In using this, each sample will be subjected to the same loading during the specimen creation resulting in a more uniform compaction of specimens.

Once the samples have been rodded the appropriate times with the Harvard Miniature Compactor, they can then be placed on a high frequency vibrating table. This table would further assist in a proper compaction of the samples as long as they are vibrated for the same times at the same frequencies. In using either of these methods or both conjunctively, the Charpy samples will be more uniform across the sample space and result in a lower coefficient of variation. The densities of each sample can also be checked as a quality control to compare the compaction of the samples. A variation in densities will signify a discrepancy in compaction and any specimens not adhering to the sample averages may be discarded.

With an optimum mix design selected in the previous section, it would be beneficial to further study “Water 2” and possibly designate it as the control mix for future parametric studies. To further understand the mechanical properties of UHPC that are associated with energy absorption, additional parametric studies should be conducted. The parameters from this study can be further studied by increasing the range of silica fume and water content. This provides the additional data necessary to see if the trends continue or if other trends develop. The sand gradation study can also be studied further. Only two mix designs are examined in this thesis in reference to gradation effect.

Additional mix designs that have varying percentages of sand gradation content will provided for further insight on the behavior attributed to grain size.

Apart from the effects of the parameters selected from this study, additional parameters can also be studied. The next logical parameter to study would be the addition of fibers to the cement matrix. A similar study on normal strength concrete by Magbool (2012) looks at the addition of poly-vinyl alcohol fibers and carbon nanofiber to increase the energy absorption. The addition of these materials would also help to increase the energy absorption for UHPC.

The final recommendation for this study is to develop full size models. In developing these models, absolute values should be obtainable. Using these absolute values, design parameters can then be developed. The current study only looks at Charpy impact values which is a relative value. Design parameters cannot be developed from these results and therefore can only be used to compare the different mix designs. A full size model would be the next step so those absolute values can then be acquired and put in design use.

BIBLIOGRAPHY

Ahlborn T. M., Harris D. K., Misson D. L., Peuse E. J., (2011). Characterization of Strength and Durability of Ultra-High-Performance Concrete Under Variable Curing Conditions. *Transportation Research Record: Journal of the Transportation Research Board.* 68-75.

Allena S., Newtson C. M., (2010). Ultra-High Strength Concrete Mixtures Using Local Materials. *National Ready Mixed Concrete Association. Concrete 2010 Sustainability Conference.*

Allena S., Newtson C. M., Weldon B. D., Jauregui D. V., (2011). Mechanical Properties and Durability Issues of Ultra-High Performance Concrete – An Overview. *International Review of Civil Engineering.* 2(4).

American Association of State Highway and Transportation Officials. (2006). AASTHO T259 Standard Method of Test for Resistance of Concrete to Chloride Ion Penetration.

ASTM International. (2012). ASTM C1609 Standard Test Method for Flexural Performance of Fiber-Reinforced Concrete (Using Beam With Third-Point Loading)

ASTM International. (2012). ASTM C672 Standard Test Method for Scaling Resistance of Concrete Surfaces Exposed to Deicing Chemicals.

ASTM International. (2012). ASTM C944 Standard Test Method for Abrasion Resistance of Concrete or Mortar Surfaces by the Rotating-Cutter Method.

ASTM International. (2013). ASTM C1202 Standard Test Method for Electrical Indication of Concrete's Ability to Resist Chloride Ion Penetration.

ASTM International. (2013). ASTM C642 Standard Test Method for Density, Absorption, and Voids in Hardened Concrete.

ASTM International. (2013). ASTM D1143/D1143M-07 Standard Test Methods for Deep Foundations Under Static Axial Compressive Load.

ASTM International. (2013). ASTM D3966-07 Standard Test Methods for Deep Foundations Under Lateral Load.

ASTM International. (2014). ASTM C1260 Standard Test Method for Potential Alkali Reactivity of Aggregates (Mortar-Bar Method).

ASTM International. (2014). ASTM C230/C230M Standard Specification for Flow Table for Use in Tests of Hydraulic Cement.

ASTM International. (2014). ASTM C469 Standard Test Method for Static Modulus of Elasticity and Poisson’s Ratio of Concrete in Compression.

ASTM International. (2014). E28 Standard Test Methods for Notched Bar Impact Testing of Metallic Material.

ASTM International. (2015). ASTM C1437 Standard Test Method for Flow of Hydraulic Cement Mortar.

ASTM International. (2015). ASTM C39 Standard Test Method for Compressive Strength of Cylindrical Concrete Specimens.

ASTM International. (2015). ASTM C666 Standard Test Method for Resistance of Concrete to Rapid Freezing and Thawing.

ASTM International. (2015). ASTM C78 Standard Test Method for Flexural Strength of Concrete (Using Simple Beam with Third-Point Loading).

ASTM International. (2016). ASTM C109 Standard Test Method for Compressive Strength of Hydraulic Cement Mortars.

British Standard. (2009). BS 12390 Testing Hardened Concrete. Tensile Splitting Strength of Test Specimens.

Collins, K.R. & Nowak, A.S. (2013). *Reliability of Structures.* 2nd ed. Boston: McGraw-Hill Higher Education.

Greaybeal B., Davis M., (2008). Cylinder or Cube: Testing of 80 to 200 MPa (11.6 to 29 ksi) Ultra-High-Performance Fiber-Reinforced Concrete. *ACI Materials.* 105(6). 603-609.

Greybeal B., (2011). Ultra-High Performance Concrete. *Federal Highway Administration.*

Greybeal B., Tanesi J., (2007). Durability of an Ultrahigh-Performance Concrete. *Journal of Materials in Civil Engineering.* 19(10). 848-854.

Huang X., He L., Ma G. W., (2011). Soil-Structure Interaction and Pulse Shape Effect on Structural Element Damage to Blast Load. *Journal of performance of Constructed Facilities.* 25(5). 400-410.

Koh C. G., Kiu Z. J., Quek S. T., (2001). Numerical and Experimental Studies of Concrete Damage Under Impact. *Magazine of Concrete Research.* 53(6). 417-427.

Krauthammer T., Bazeos N., Holmquist T. J., (1986). Modified SDOF Analysis of RC Box-Type Structures. *Journal of Structural Engineering.* 112(4). 726-744.

Ma G. W., Huang X., Li J. C., (2010). Simplified Damage Assessment Method for Buried Structures against External Blast Load. *Journal of Structural Engineering.* 136(5). 603-612.

Magbool H., (2012). Impact Resistance of Fiber-Reinforced Concrete Material. *Idaho State University.* Thesis.

Magnusson J., Hallgren M., Ansell A., (2014). Shear in Concrete Structures Subject to Dynamic Loads. *Structural Concrete.* 15(1). 56-64.

Magureanu C., Sosa I., Negrutiu C., Bogdan H., (2012). Mechanical Properties and Durability of Ultra-High-Performance Concrete. *ACI Materials Journal.* 109(2). 177-184

Naito C. J., Wheaton K. P., (2006). Blast Assessment of Load-Bearing Reinforced Concrete Shear Walls. *Practice Periodical on Structural Design and Construction.* 11(2). 112-121

Prem P. R., Bharatkumar B.H., Iyer N. R., (2012). Mechanical Properties of Ultra High Performance Concrete. *International Scholarly and Scientific Research & Innovation.* 6(8). 1676-1685.

Suaris W., Shah S. P., (1983). Properties of Concrete Subjected to Impact. *Journal of Structural Engineering.* 109(7). 1727-1741.

Suleiman M. T., Voort T. V., Sritharan S., (2010). Behavior of Driven Ultrah-High-Performance Concrete H-Piles Subjected to Vertical and Lateral Loadings. *Journal of Geotechnical and Geoenvironmental Engineering.* 1403-1413

Tam C. M., Tam V. W. Y., Ng K. M., (2010). Optimal Conditions for Producing Reactive Powder Concrete. *Magazine of Concrete Research.* 62(10). 701-716

Wille K., Naaman A. E., Parra-Montesinos G. J., (2011). Ultra-High Performance Concrete with Compressive Strength Exceeding 150 MPa (22 ksi): A Simpler Way. *ACI Materials Journal.* 108(1). 46-54

Xu B., Toutanji H., Gilber J., (2009). Impact Resistance of Poly(vinyl alcohol) Fiber Reinforced High-Performance Organic Aggregate Cementitious Material. *Cement and Concrete Research.* 40. 347-351.

APPENDICES

Appendix A: Materials Specifications

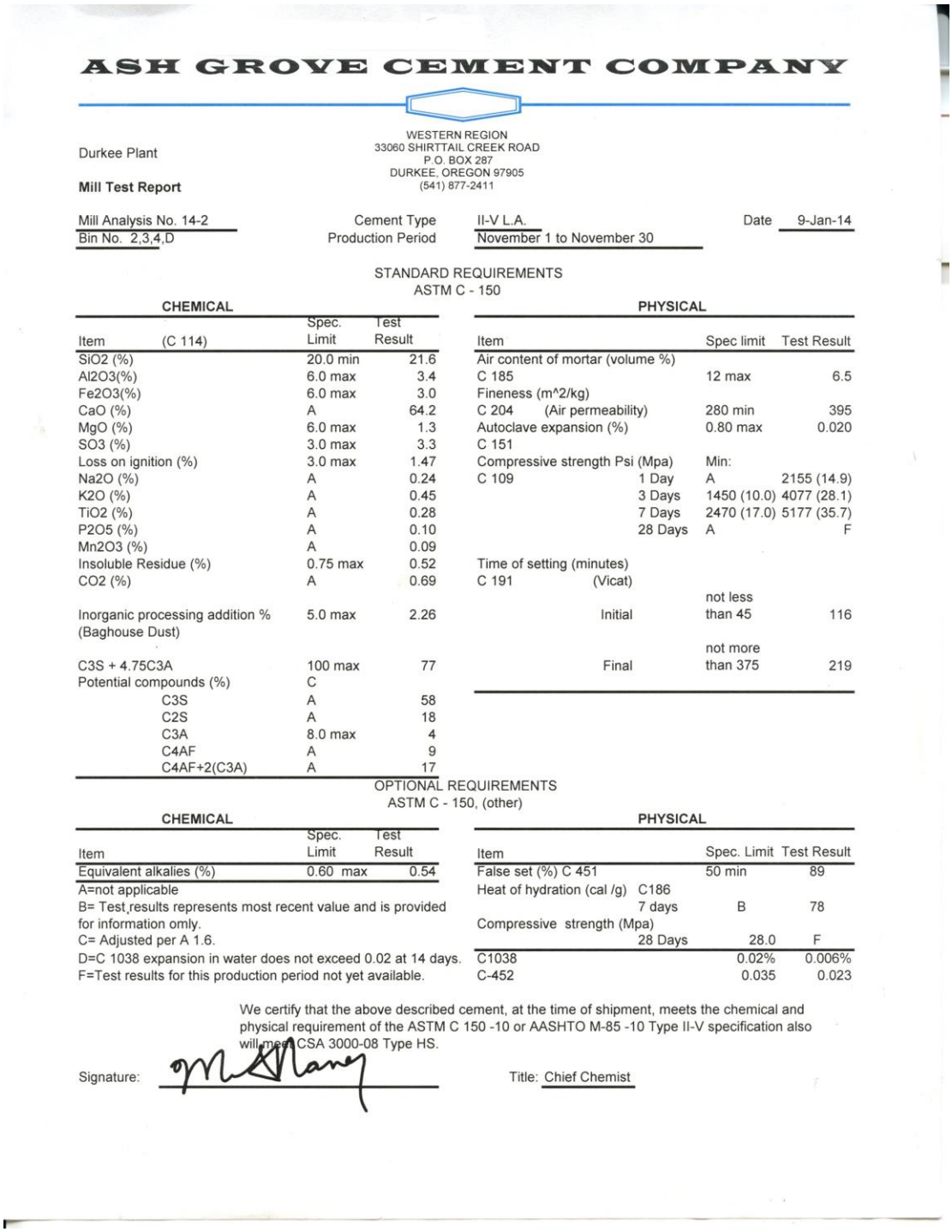

ASH GROVE CEMENT COMPANY

WESTERN REGION
33060 SHIRTTAIL CREEK ROAD
P.O. BOX 287
DURKEE, OREGON 97905
(541) 877-2411

Durkee Plant

Mill Test Report

Mill Analysis No. 14-2 — Cement Type II-V L.A. — Date 9-Jan-14
Bin No. 2,3,4,D — Production Period November 1 to November 30

STANDARD REQUIREMENTS
ASTM C - 150

CHEMICAL

Item (C 114)	Spec. Limit	Test Result
SiO2 (%)	20.0 min	21.6
Al2O3(%)	6.0 max	3.4
Fe2O3(%)	6.0 max	3.0
CaO (%)	A	64.2
MgO (%)	6.0 max	1.3
SO3 (%)	3.0 max	3.3
Loss on ignition (%)	3.0 max	1.47
Na2O (%)	A	0.24
K2O (%)	A	0.45
TiO2 (%)	A	0.28
P2O5 (%)	A	0.10
Mn2O3 (%)	A	0.09
Insoluble Residue (%)	0.75 max	0.52
CO2 (%)	A	0.69
Inorganic processing addition % (Baghouse Dust)	5.0 max	2.26
C3S + 4.75C3A	100 max	77
Potential compounds (%)	C	
C3S	A	58
C2S	A	18
C3A	8.0 max	4
C4AF	A	9
C4AF+2(C3A)	A	17

PHYSICAL

Item		Spec limit	Test Result
Air content of mortar (volume %)			
C 185		12 max	6.5
Fineness (m^2/kg)			
C 204	(Air permeability)	280 min	395
Autoclave expansion (%)		0.80 max	0.020
C 151			
Compressive strength Psi (Mpa)		Min:	
C 109	1 Day	A	2155 (14.9)
	3 Days	1450 (10.0)	4077 (28.1)
	7 Days	2470 (17.0)	5177 (35.7)
	28 Days	A	F
Time of setting (minutes)			
C 191	(Vicat)		
	Initial	not less than 45	116
	Final	not more than 375	219

OPTIONAL REQUIREMENTS
ASTM C - 150, (other)

CHEMICAL

Item	Spec. Limit	Test Result
Equivalent alkalies (%)	0.60 max	0.54

PHYSICAL

Item		Spec. Limit	Test Result
False set (%) C 451		50 min	89
Heat of hydration (cal /g)	C186		
	7 days	B	78
Compressive strength (Mpa)			
	28 Days	28.0	F
C1038		0.02%	0.006%
C-452		0.035	0.023

A=not applicable
B= Test results represents most recent value and is provided for information omly.
C= Adjusted per A 1.6.
D=C 1038 expansion in water does not exceed 0.02 at 14 days.
F=Test results for this production period not yet available.

We certify that the above described cement, at the time of shipment, meets the chemical and physical requirement of the ASTM C 150 -10 or AASHTO M-85 -10 Type II-V specification also will meet CSA 3000-08 Type HS.

Signature: _____ Title: Chief Chemist

Figure A.1: Portland Cement Data Sheet

BASF
The Chemical Company

3 | 03 30 00 Cast-in-Place Concrete | 03 40 00 Precast Concrete | 03 70 00 Mass Concrete | Product Data

RHEOMAC® SF 100

Densified Silica Fume Mineral Admixture

Description

Rheomac SF 100 dry, densified silica fume mineral admixture is formulated to produce extremely strong, durable concrete or mortar possessing special performance qualities. It maximizes concrete service life by providing superior resistance to attack from damaging environmental forces. Rheomac SF 100 silica fume admixture meets the requirements of ASTM C 1240, *Standard Specification for Silica Fume used in Cementious Mixtures.*

Applications

Recommended for use in:

- Steel-reinforced concrete structures or wet shotcrete applications exposed to deicing or airborne salts
- Parking structures, bridge decks, marine structures, mines and tunnels
- Any construction project requiring the protection provided by highly durable, low permeability concrete
- Projects requiring high-strength/high-performance concrete for reducing member size, increasing span lengths, improving structural economics and meeting other high-performance structural requirements

Features

- Added cohesiveness
- Reduced bleeding
- Enhanced performance

Benefits

- Increased concrete service life
- Improved strength
- Increased modulus of elasticity
- Reduced permeability thereby increasing durability
- Increased resistance to sulfate attack
- Increased resistance to alkali-silica reactivity

Performance Characteristics

Permeability: Rheomac SF 100 silica fume admixture is a micro-filling material that physically fills the voids between cement particles. Rheomac SF 100 silica fume admixture dramatically lowers permeability and reduces the size and number of capillaries that allow contaminants to enter the matrix.

Rapid Chloride Permeability ***Test Typical Compressive Strengths***

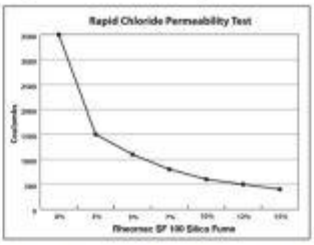

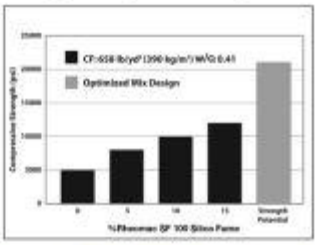

Compressive Strength: As a pozzolan, Rheomac SF 100 silica fume admixture reacts chemically within a cementitious matrix to increase the amount of calcium silicate hydrate (CSH gel) that is formed. The CSH gel is the bonding agent that holds the matrix of a cementitious mixture together in the hardened state. The additional CSH gel increases strength and decreases permeability.

Specific Gravity: The specific gravity of Rheomac SF 100 silica fume admixture is 2.2.

Master Builders

Figure A.2.a: Silica Fume Date Sheet

Product Data: RHEOMAC® SF 100

Guidelines for Use

Dosage: Rheomac SF 100 silica fume admixture is recommended for use in concrete and wet shotcrete applications at an addition dosage of 5-15% by mass of cement.

Dispensing and Mixing: For concrete and wet shotcrete, Rheomac SF 100 silica fume admixture is batched at the concrete production plant in a manner similar to that for cement or other cementitious materials such as fly ash. It may be batched in a central or truck mixer. Follow the procedures outlined in ASTM C 94/C 94M, *Standard Specification for Ready-Mixed Concrete* or refer to the *Silica Fume Association Users Manual* for specific batching and mixing instructions.

Product Notes

Corrosivity – Non-Chloride, Non-Corrosive: Rheomac SF 100 silica fume admixture will neither initiate nor promote corrosion of reinforcing or prestressing steel embedded in concrete or of galvanized steel floor and roof systems. Neither calcium chloride nor other chloride-based ingredients are used in the manufacture of this silica fume.

Compatibility: Rheomac SF 100 silica fume admixture can be used with portland cements approved under ASTM, AASHTO or CRD specifications. It is compatible with most concrete admixtures, including all BASF Construction Chemicals admixtures. Rheomac SF 100 silica fume admixture is recommended for use with high-range water-reducing admixtures, such as the Glenium® series, for maximum workability while maintaining a low water-cementitious materials ratio.

Handling and Storage

Rheomac SF 100 silica fume admixture stores, handles and dispenses similar to cement or fly ash. In bulk, Rheomac SF 100 silica fume admixture may be stored in a silo. Refer to the *Silica Fume Association Users Manual* for information on the appropriate set up for pumping and handling silica fume into silos. Packaged Rheomac SF 100 admixture must be stored in a dry area. Rheomac SF 100 silica fume admixture requires no special dispensing equipment.

Shelf Life: Rheomac SF 100 admixture has a minimum shelf life of 24 months. Depending on storage conditions, the shelf life may be greater than stated. Please contact your BASF Construction Chemicals representative regarding suitability for use and dosage recommendations if the shelf life of Rheomac SF 100 admixture has been exceeded.

Packaging

Rheomac SF 100 silica fume admixture is available in 25 lb (11.6 kg) shreddable bags, 2,000 lb (907 kg) bulk bags or by bulk delivery.

Related Document

Silica Fume Association Users Manual
Material Safety Data Sheet: Rheomac SF 100 silica fume admixture.

Additional Information

For additional information on Rheomac SF 100 silica fume admixture or its use in developing concrete mixtures with special performance characteristics, contact your BASF Construction Chemicals representative.

The Admixture Systems business of BASF Construction Chemicals is a leading provider of innovative additives for specialty concrete used in the ready mix, precast, manufactured concrete products, underground construction and paving markets throughout the NAFTA region. The Company's respected Master Builders brand products are used to improve the placing, pumping, finishing, appearance and performance characteristics of concrete.

BASF Construction Chemicals, LLC
Admixture Systems

www.masterbuilders.com
United States 23700 Chagrin Boulevard, Cleveland, Ohio 44122-5544 ■ Tel: 800 628-9990 ■ Fax: 216 839-8821
Canada 1800 Clark Boulevard, Brampton, Ontario L6T 4M7 ■ Tel: 800 387-5862 ■ Fax: 905 792-0651
® Construction Research & Technology GMBH

Master Builders

Figure A.2.b: Silica Fume Date Sheet

BASF
We create chemistry

3	03 30 00	Cast-in-Place Concrete
	03 40 00	Precast Concrete
	03 70 00	Mass Concrete
4	04 05 16	Masonry Grouting

MasterGlenium® 3030

Full-Range Water-Reducing Admixture

Formerly Glenium 3030 NS®

Description

MasterGlenium 3030 ready-to-use full-range water-reducing admixture is a patented new generation of admixture based on polycarboxylate chemistry. MasterGlenium 3030 admixture is very effective in producing concretes with different levels of workability including applications that require the use of self-consolidating concrete (SCC). MasterGlenium 3030 admixture meets ASTM C 494/C 494M requirements for Type A, water-reducing, and Type F, high-range water-reducing, admixtures.

Applications

Recommended for use in:

- Concrete where high flowability, high-early and ultimate strengths and increased durability are needed
- Self-consolidating concrete
- Concrete where normal, mid-range, or high-range water-reduction is desired
- Concrete where normal setting times are required
- Strength-on-demand concrete, such as 4x4™ Concrete
- Pervious concrete
- Self-consolidating grout

Features

- Dosage flexibility for normal, mid- and high-range water reduction
- Reduced water content for a given slump
- Produces cohesive and non-segregating concrete mixture
- Increased compressive strength and flexural strength performance at all ages
- Providing faster setting times and strength development
- Enhanced finishability and pumpability

Benefits

- Providing economic benefits to the entire construction team through higher productivity and reduced variable costs

Performance Characteristics

The dosage flexibility of MasterGlenium 3030 admixture allows it to be used as a normal, mid-range and high-range water reducer.

Mixture Data: 600 lb/yd³ of Type I cement (360 kg/m³); slump, 8.5-9.25 in. (210-235 mm); non-air-entrained concrete; dosage rate adjusted to obtain 25-30% water reduction.

MASTER® BUILDERS SOLUTIONS

Figure A.3.a: Master Glenium Data Sheet

Setting Time

Mixture	Initial Set (h:min)	Difference (h:min)
Plain	4:24	–
Conventional high-range water-reducer	6:00	+ 1.36
MasterGlenium 3030 admixture	5:00	+0.36

Compressive Strength

	1 Day		7 Days	
Mixture	psi	MPa	psi	MPa
Plain	1700	12	4040	28
Conventional high-range water-reducer	3460	24	6380	44
MasterGlenium 3030 admixture	4120	28	7580	52

Slump Retention - in. (mm)

	Minutes		
Mixture	15	30	45
Plain	8.5 (215)	8.5 (215)	7.5 (200)
Conventional high-range water-reducer	8.5 (215)	4.25 (110)	3.5 (90)
MasterGlenium 3030 admixture	9.25 (235)	9.25 (235)	8.25 (210)

Rate of Hardening: MasterGlenium 3030 admixture is formulated to produce normal setting characteristics throughout its recommended dosage range. Setting time of concrete is influenced by the chemical and physical composition of the basic ingredients of the concrete, temperature of the concrete and ambient conditions. Trial mixtures should be made with actual job materials to determine the dosage required for a specified setting time and a given strength requirement.

Guidelines for Use

Dosage: MasterGlenium 3030 admixture has a recommended dosage range of up to 3 fl oz/cwt (195 mL/100 kg) for Type A applications, 3-6 fl oz/cwt (195-390 mL/100 kg) for mid-range use and up to 18 fl oz/cwt (1,170 mL/100 kg) for Type F applications. The dosage range is applicable to most mid- to high-range concrete mixtures using typical concrete ingredients. However, variations in job conditions and concrete materials, such as silica fume, may require dosages outside the recommended range. In such cases, contact your local sales representative.

Mixing: MasterGlenium 3030 admixture can be batched with the initial mixing water or as a delayed addition. However, optimum water reduction is generally obtained with a delayed addition.

Product Notes

Corrosivity – Non-Chloride, Non-Corrosive: MasterGlenium 3030 admixture will neither initiate nor promote corrosion of reinforcing steel embedded in concrete, prestressed concrete or of galvanized steel floor and roof systems. Neither calcium chloride nor other chloride-based ingredients are used in the manufacture of MasterGlenium 3030 admixture.

Compatibility: MasterGlenium 3030 admixture is compatible with most admixtures used in the production of quality concrete, including normal, mid-range and high-range water-reducing admixtures, air-entrainers, accelerators, retarders, extended set control admixtures, corrosion inhibitors, and shrinkage reducers.

Do not use MasterGlenium 3030 admixture with admixtures containing beta-naphthalene-sulfonate. Erratic behaviors in slump, slump flow, and pumpability may be experienced.

For directions on the proper evaluation of MasterGlenium 3030 admixture in specific applications, contact your local sales representative.

Figure A.3.b: Master Glenium Data Sheet

Storage and Handling

Storage Temperature: MasterGlenium 3030 admixture should be stored above freezing temperatures. If MasterGlenium 3030 admixture freezes, thaw at 45 °F (7 °C) or above and completely reconstitute by mild mechanical agitation. **Do not use pressurized air for agitation.**

Shelf Life: MasterGlenium 3030 admixture has a minimum shelf life of 12 months. Depending on storage conditions, the shelf life may be greater than stated. Please contact your local sales representative regarding suitability for use and dosage recommendations if the shelf life of MasterGlenium 3030 admixture has been exceeded.

Packaging

MasterGlenium 3030 admixture is supplied in 55 gal (208 L) drums, 275 gal (1040 L) totes and by bulk delivery.

Related Documents

Safety Data Sheets: MasterGlenium 3030 admixture

Additional Information

For additional information on MasterGlenium 3030 admixture or its use in developing concrete mixes with special performance characteristics, contact your local sales representative.

The Admixture Systems business of BASF's Construction Chemicals division is the leading provider of solutions that improve placement, pumping, finishing, appearance and performance characteristics of specialty concrete used in the ready-mixed, precast, manufactured concrete products, underground construction and paving markets. For over 100 years we have offered reliable products and innovative technologies, and through the Master Builders Solutions brand, we are connected globally with experts from many fields to provide sustainable solutions for the construction industry.

Limited Warranty Notice

BASF warrants this product to be free from manufacturing defects and to meet the technical properties on the current Technical Data Guide, if used as directed within shelf life. Satisfactory results depend not only on quality products but also upon many factors beyond our control. BASF MAKES NO OTHER WARRANTY OR GUARANTEE, EXPRESS OR IMPLIED, INCLUDING WARRANTIES OF MERCHANTABILITY OR FITNESS FOR A PARTICULAR PURPOSE WITH RESPECT TO ITS PRODUCTS. The sole and exclusive remedy of Purchaser for any claim concerning this product, including but not limited to, claims alleging breach of warranty, negligence, strict liability or otherwise, is shipment to purchaser of product equal to the amount of product that fails to meet this warranty or refund of the original purchase price of product that fails to meet this warranty, at the sole option of BASF. Any claims concerning this product must be received in writing within one (1) year from the date of shipment and any claims not presented within that period are waived by Purchaser. BASF WILL NOT BE RESPONSIBLE FOR ANY SPECIAL, INCIDENTAL, CONSEQUENTIAL (INCLUDING LOST PROFITS) OR PUNITIVE DAMAGES OF ANY KIND.

Purchaser must determine the suitability of the products for the intended use and assumes all risks and liabilities in connection therewith. This information and all further technical advice are based on BASF's present knowledge and experience. However, BASF assumes no liability for providing such information and advice including the extent to which such information and advice may relate to existing third party intellectual property rights, especially patent rights, nor shall any legal relationship be created by or arise from the provision of such information and advice. BASF reserves the right to make any changes according to technological progress or further developments. The Purchaser of the Product(s) must test the product(s) for suitability for the intended application and purpose before proceeding with a full application of the product(s). Performance of the product described herein should be verified by testing and carried out by qualified experts.

* Glenium 3030 NS became MasterGlenium 3030 under the Master Builders Solutions brand, effective January 1, 2014.

BASF Corporation
Admixture Systems
www.master-builders-solutions.basf.us

United States
23700 Chagrin Boulevard
Cleveland, Ohio 44122-5544
Tel: 800 628-9990 • Fax: 216 839-8821

Canada
1800 Clark Boulevard
Brampton, Ontario L6T 4M7
Tel: 800 387-5892 • Fax: 905 792-0651

Figure A.3.c: Master Glenium Data Sheet

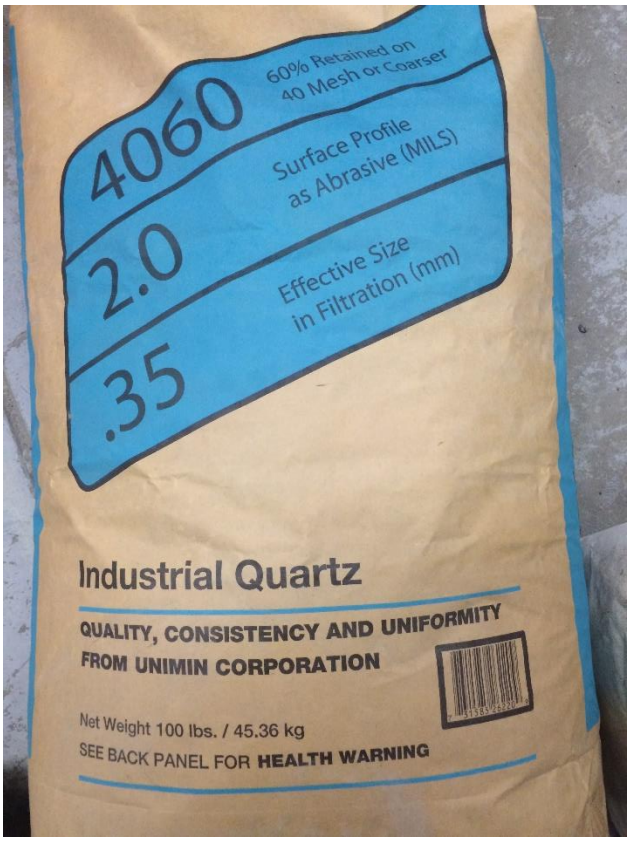

Figure A.4: Crushed Quartz Sand

Appendix B: Mix Design Proportions

Appendix B.1: Trial Mix Proportions

Table B.1: Mix Proportions - Trial Design 1: Allena and Newson (2010)

Date Cast: 4/16/15			Date to Test: 5/14/15			
Allena - 1						
5 - 4x8 cylinders	lb/yd3	lbs	grams			
Cement	1500	20.20057	9162.817			
Silica Fume	375	5.050143	2290.704			
Fine Sand	1411	19.002	8619.156			
Water	375	5.050143	3863.704		w/c	0.42
HRWRA (gal)	6	0.080802	16	(oz)	w/b	0.34

Table B.2: Mix Proportions - Trial Design 2: Tam and others (2010)

Date Cast: 4/24/15			Date to Test: 5/22/15			
Tam - 1						
5 - 4x8 cylinders	kg/m3	lb/yd3	lbs	grams		
Cement	761	1282.706	17.27426	7835.466		
Silica Fume	247	416.3316	5.606757	2543.18		
Fine Sand	1316	2218.188	29.87244	13549.9		
Water	202	340.4817	4.585283	4019.848	w/c	0.51
HRWRA (gal)	19	32.02551	0.431289	195.6292	w/b	0.39

Table B.3: Mix Proportions - Trial Design 3: Allena and Others (2010)

Date Cast: 4/31/15			Date to Test: 5/29/15			
Allena - 2			*Tested on 5/22/15 (21 Day Strength)			
5 - 4x8 cylinders	lb/yd3	lbs	grams			
Cement	1500	21.61134	9802.73			
Silica Fume	375	5.402834	2450.682			
Fine Sand	1411	20.32906	9221.101			
Water	375	5.402834	2450.682		w/c	0.25
HRWRA (gal)	6	0.086445	11.065	(oz)	w/b	0.20

Table B.4: Mix Proportions - Trial Design 4: Allena and Others (2010)

Date Cast: 9/22/15			Date to Test: 10/20/2015			
Allena -3						
5 - 4x8 cylinders	lb/yd3	lbs	grams			
Cement	1500	21.61134	9802.73			
Silica Fume	375	5.402834	2450.682			
Fine Sand	1411	20.32906	9221.101			
Water	375	5.402834	2450.682		w/c	0.25
HRWRA (gal)	6	0.086445	11.065	(oz)	w/b	0.20

Table B.5: Mix Proportions - Trial Design 5: Allena and Others (2010)

Date Cast: 10/22/15			Date to Test: 11/20/2015			
Allena						
9 - 2"x2" cubes, 9 Charpy						
	lb/yd3	lbs	grams			
Cement	1500	3.993056	1811.218			
Silica Fume	375	0.998264	452.8045			
Fine Sand	1411	3.756134	1703.752			
Water	375	0.998264	407.5		w/c	0.22
HRWRA (gal)	6	0.015972	9	oz	w/b	0.18

Appendix B.2: Mix Designs

Table B.6: Mix Proportions - Control Mix

Date Cast: 10/21/15			Date to Test: 11/19/2015			
Allena						
9 - 2"x2" cubes, 9 Charpy					**Control**	
	lb/yd3	lbs	grams			
Cement	1500	4.340278	1968.715			
Silica Fume	375	1.085069	492.1788			
Fine Sand	1411	4.082755	1851.905	(sieved through #30)		
Water	375	1.085069	492.1788		w/c	0.25
HRWRA (gal)	6	0.017361	2		w/b	0.20

Table B.7: Mix Proportions - Silica Fume 1

Date Cast: 12/15/15			Date to Test: 1/12/2016			
Allena						
9 - 2"x2" cubes, 12 Charpy					**SF 1**	
	lb/yd3	lbs	grams			
Cement	1575	4.658565	2113.088			
Silica Fume	300	0.887346	402.4929			
Fine Sand	1411	4.173483	1893.058			
Water	375	1.109182	503.1161		w/c	0.24
HRWRA (gal)	6	0.017747	2.271605		w/b	0.20

Table B.8: Mix Proportions - Silica Fume 2

Date Cast: 12/15/15			Date to Test: 1/12/2016			
Allena						
9 - 2"x2" cubes, 12 Charpy					**SF 2**	
	lb/yd3	lbs	grams			
Cement	1537.5	4.547647	2062.776	2515.581		
Silica Fume	337.5	0.998264	452.8045		0.220	
Fine Sand	1411	4.173483	1893.058			
Water	375	1.109182	503.1161		w/c	0.24
HRWRA (gal)	6	0.017747	2.271605		w/b	0.20

Table B.9: Mix Proportions - Silica Fume 3

Date Cast: 12/16/15			Date to Test: 1/13/2016			
Allena						
9 - 2"x2" cubes, 12 Charpy					**SF 3**	
	lb/yd3	lbs	grams			
Cement	1462.5	4.32581	1962.153	2515.581		
Silica Fume	412.5	1.2201	553.4277		0.282	
Fine Sand	1411	4.173483	1893.058			
Water	375	1.109182	503.1161		w/c	0.26
HRWRA (gal)	6	0.017747	3.5		w/b	0.20

Table B.10: Mix Proportions - Silica Fume 4

Date Cast: 12/16/15			Date to Test: 1/13/2016			
Allena						
9 - 2"x2" cubes, 12 Charpy					**SF 4**	
	lb/yd3	lbs	grams			
Cement	1425	4.214892	1911.841	2515.581		
Silica Fume	450	1.331019	603.7394		0.316	
Fine Sand	1411	4.173483	1893.058			
Water	375	1.109182	503.1161		w/c	0.26
HRWRA (gal)	6	0.017747	3.5		w/b	0.20

Table B.11: Mix Proportions - Water 1

Date Cast: 12/17/15			Date to Test: 1/14/2016			
Allena						
9 - 2"x2" cubes, 12 Charpy					**Water 1**	
	lb/yd3	lbs	grams			
	lb/yd3	lbs	grams			
Cement	1500	4.436728	2012.465			
Silica Fume	375	1.109182	503.1161			
Fine Sand	1411	4.173483	1893.058			
Water	375	1.109182	603.7394		w/c	0.30
HRWRA (gal)	6	0.017747	2.158025		w/b	0.24

Table B.12: Mix Proportions - Water 2

Date Cast: 12/17/15			Date to Test: 1/14/2016			
Allena						
9 - 2"x2" cubes, 12 Charpy					**Water 2**	
	lb/yd3	lbs	grams			
	lb/yd3	lbs	grams			
Cement	1500	4.436728	2012.465			
Silica Fume	375	1.109182	503.1161			
Fine Sand	1411	4.173483	1893.058			
Water	375	1.109182	553.4277		w/c	0.275
HRWRA (gal)	6	0.017747	2.214815	(oz)	w/b	0.22

Table B.13: Mix Proportions - Water 3

Date Cast: 12/18/15			Date to Test: 1/15/2016			
Allena						
9 - 2"x2" cubes, 12 Charpy					**Water 3**	
	lb/yd3	lbs	grams			
	lb/yd3	lbs	grams			
Cement	1500	4.436728	2012.465			
Silica Fume	375	1.109182	503.1161			
Fine Sand	1411	4.173483	1893.058			
Water	375	1.109182	452.8045		w/c	0.23
HRWRA (gal)	6	0.017747	2.328395	(oz)	w/b	0.18

Table B.14: Mix Proportions – Water 4

Date Cast: 12/18/15			Date to Test: 1/15/2016			
Allena						
9 - 2"x2" cubes, 12 Charpy					**Water 4**	
	lb/yd3	lbs	grams			
	lb/yd3	lbs	grams			
Cement	1500	4.436728	2012.465			
Silica Fume	375	1.109182	503.1161			
Fine Sand	1411	4.173483	1893.058			
Water	375	1.109182	402.4929		w/c	0.20
HRWRA (gal)	6	0.017747	2.385185	(oz)	w/b	0.16

Table B.15: Mix Proportions - Sieve 1

Date Cast: 12/19/15			Date to Test: 1/16/2016			
Allena						
9 - 2"x2" cubes, 12 Charpy					**Sieve 1**	
	lb/yd3	lbs	grams			
Cement	1500	4.436728	2012.465			
Silica Fume	375	1.109182	503.1161			
Fine Sand	1411	4.173483	1893.058	30+		
Water	375	1.109182	503.1161			
HRWRA (gal)	6	0.017747	2.271605	(oz)		

Table B.16: Mix Proportions – Sieve 2

Date Cast: 12/19/15			Date to Test: 1/16/2016			
Allena						
9 - 2"x2" cubes, 12 Charpy					**Sieve 2**	
	lb/yd3	lbs	grams			
Cement	1500	4.436728	2012.465			
Silica Fume	375	1.109182	503.1161			
Fine Sand	705.5	2.086742	946.529	30+		
Fine Sand	705.5	2.086742	946.529	30-		
Water	375	1.109182	503.1161			
HRWRA (gal)	6	0.017747	2.271605	(oz)		

Appendix C: Compression Results

Appendix C.1: Trial Mix Designs

Table C.1: Compression Results - Trial 1

Specimen	D_1 (in)	D_2 (in)	D_3 (in)	Avg (in)	Area (in^2)	Load (lbs)	Stress (psi)
1	3.98	4.15	4.25	4.126666667	13.37484203	103670	7751.1
2	4.1	4.25	3.98	4.11	13.26702432	106590	8034.2
3	3.98	3.98	4.05	4.003333333	12.58732329	77980	6195.1
4	3.98	4.05	4.25	4.093333333	13.15964293	108060	8211.5
5	4	4.05	4.05	4.033333333	12.77668279	98220	7687.4
						Average:	7575.9

Table C.2: Compression Results - Trial 2

Specimen	D_1 (in)	D_2 (in)	D_3 (in)	Avg (in)	Area (in^2)	Load (lbs)	Stress (psi)
1	4.005	3.997	3.969	3.990333333	12.50570655	93020	7438.2
2	3.963	3.984	3.997	3.981333333	12.44935816	58090	4666.1
3	3.993	4.013	4.058	4.021333333	12.70076934	70080	5517.8
4	4.081	3.96	3.958	3.999666667	12.56427631	90510	7203.8
5	3.991	3.982	3.98	3.984333333	12.46812682	93460	7495.9
						Average:	6464.4

Table C.3: Compression Results - Trial 3

Specimen	D_1 (in)	D_2 (in)	D_3 (in)	Avg (in)	Area (in^2)	Load (lbs)	Stress (psi)
1	3.089	3.093	3.074	3.085333333	7.476426425	-	-
2	3.07	3.054	3.039	3.054333333	7.326941854	22560	3079.0
3	3.071	3.074	3.081	3.075333333	7.428040662	19940	2684.4
4	3.096	3.093	3.079	3.089333333	7.495824713	27920	3724.7
5	3.066	3.068	3.066	3.066666667	7.386233394	25780	3490.3
						Average:	3244.6

Table C.4: Compression Results - Trial 4

Specimen	H (in)	D_1 (in)	D_2 (in)	D_3 (in)	Avg (in)	Area (in^2)	Load (lbs)	Stress (psi)
1	8.146	4.049	4.003	3.969	4.007	12.61039	133340	10573.8
2	8.119	3.977	3.968	3.959	3.968	12.36611	170530	13790.1
3	8.187	4.022	3.991	3.968	3.993667	12.52661	128340	10245.4
4	8.2	3.948	3.94	3.964	3.950667	12.25831	131790	10751.1
5	8.18	3.992	4.013	3.969	3.991333	12.51198	144050	11513.0
							Average:	11374.7

Table C.5: Compression Results - Trial 5

Specimen	Average length	Average base	Average height	Max Load (ft-lb)	Compressive Strength (psi)
1	2.037	2.023	2.038	263.44	14933.8
2	2.017	2.032	2.032	262.33	9114.5
3	2.019	2.021	2.027	261.14	15000.4
4	2.026	2.056	2.014	261.77	9194.8
5	2.032	2.039	2.029	260.57	11709.6
6	2.037	2.052	2.027	262.4	13920.1
7	2.037	2.043	2.039	267.43	12130.9
8	2.026	2.035	2.040	263.39	10990.9
9	2.027	2.048	2.051	265.63	15872.3
				Average:	12540.8

Appendix C.2: Compression Results

Table C.6: Compression Results – Control

Specimen	Average length	Average base	Average height	Max Load (lbs)	Compressive Strength (psi)
1	2.018	2.044	2.006	90310	22021.8
2	2.041	2.037	2.022	74950	18197.0
3	2.014	2.020	2.009	64800	15965.1
4	2.000	2.050	2.012	88610	21479.7
5	2.024	2.047	2.050	98820	23552.9
6	2.008	2.017	2.019	72680	17850.3
7	2.024	2.046	2.032	86460	20799.7
8	2.044	2.058	2.044	79280	18843.7
9	2.047	2.020	2.057	100230	24121.9
				Average:	20314.7

Table C.7: Compression Results - Silica Fume 1

Specimen	Average length	Average base	Average height	Max Load (lbs)	Compressive Strength (psi)
1	2.008	2.044	2.008	63350	15432.3
2	2.005	2.029	2.025	67750	16483.9
3	2.012	2.032	2.001	72950	17938.3
4	2.039	2.066	2.009	54960	13245.8
5	2.017	2.055	2.021	50440	12145.0
6	1.995	2.039	2.007	77160	18848.8
7	2.036	2.046	2.016	76410	18527.8
8	2.063	2.058	2.008	65350	15816.4
9	2.034	2.014	2.033	70730	17274.6
				Average:	16190.3

Table C.8: Compression Results - Silica Fume 2

Specimen	Average length	Average base	Average height	Max Load (lbs)	Compressive Strength (psi)
1	2.003	2.012	2.009	55410	13710.5
2	2.029	2.016	2.037	59760	14549.8
3	2.000	2.040	2.011	54620	13318.4
4	2.019	2.043	2.000	87280	21360.7
5	2.025	2.043	2.027	77790	18781.5
6	2.009	2.048	2.009	57540	13982.6
7	2.007	2.035	2.012	64810	15828.8
8	2.009	2.049	2.033	44380	10657.4
9	2.013	2.044	2.019	69530	16851.0
				Average:	15449.0

Table C.9: Compression Results - Silica Fume 3

Specimen	Average length	Average base	Average height	Max Load (lbs)	Compressive Strength (psi)
1	2.026	2.033	2.019	79510	19367.6
2	2.012	2.036	2.005	74220	18184.4
3	2.005	2.011	2.023	72900	17925.2
4	2.032	2.025	2.025	63550	15497.6
5	2.035	2.021	2.032	91500	22280.8
6	2.038	2.022	2.015	86360	21199.6
7	2.029	2.019	2.006	77980	19253.8
8	2.030	2.028	2.003	89770	22099.4
9	2.019	2.023	2.003	89620	22124.4
				Average:	19770.3

Table C.10: Compression Results - Silica Fume 4

Specimen	Average length	Average base	Average height	Max Load (lbs)	Compressive Strength (psi)
1	2.018	2.032	2.006	65170	15993.2
2	2.019	2.022	2.006	55230	13614.2
3	2.016	2.033	2.013	69810	17052.7
4	2.023	2.032	1.997	50080	12337.3
5	2.016	2.019	2.041	47540	11536.6
6	2.033	2.026	2.026	67040	16327.2
7	2.011	2.030	2.008	75380	18498.6
8	2.012	2.055	2.015	36730	8870.2
9	2.039	2.036	2.012	67750	16536.0
				Average:	14529.6

Table C.11: Compression Results - Water 1

Specimen	Average length	Average base	Average height	Max Load (lbs)	Compressive Strength (psi)
1	2.021	2.025	1.987	72300	17971.6
2	2.020	2.022	2.017	50590	12402.4
3	2.021	2.039	2.009	68380	16692.9
4	2.010	2.023	2.006	66230	16320.3
5	2.028	2.027	2.018	77430	18926.2
6	2.017	2.022	2.011	59850	14718.7
7	2.020	2.039	1.998	61690	15143.2
8	2.028	2.024	2.014	75250	18460.2
9	2.013	2.028	2.000	74260	18311.7
				Average:	16549.7

Table C.12: Compression Results - Water 2

Specimen	Average length	Average base	Average height	Max Load (lbs)	Compressive Strength (psi)
1	2.011	2.029	2.010	63370	15543.5
2	2.016	2.028	2.031	80380	19521.5
3	2.020	2.022	2.022	74710	18270.3
4	2.002	2.031	2.001	68880	16943.1
5	2.014	2.031	2.004	67970	16699.7
6	2.026	2.042	2.025	70420	17027.2
7	2.011	2.034	2.008	87650	21463.9
8	2.022	2.026	2.024	80900	19732.0
9	2.016	2.030	2.004	86850	21348.9
				Average:	18505.6

Table C.13: Compression Results - Water 3

Specimen	Average length	Average base	Average height	Max Load (lbs)	Compressive Strength (psi)
1	2.014	2.050	2.004	90100	21931.7
2	2.018	2.042	2.025	87410	21138.8
3	2.016	2.033	2.003	82120	20159.8
4	2.009	2.034	2.013	102140	24946.1
5	2.018	2.038	2.030	103090	24918.2
6	2.021	2.045	2.018	83260	20175.3
7	2.011	2.029	2.020	94860	23144.6
8	2.024	2.038	2.021	70460	17112.6
9	2.011	2.036	2.001	65730	16133.9
				Average:	21073.4

Table C.14: Compression Results - Sieve 1

Specimen	Average length	Average base	Average height	Max Load (lbs)	Compressive Strength (psi)
1	2.011	2.033	1.999	88120	21683.3
2	2.017	2.039	2.027	87590	21189.1
3	2.016	2.041	2.005	67230	16426.1
4	2.010	682.016	2.008	77790	56.8
5	2.019	2.033	2.034	83590	20214.6
6	2.024	2.035	2.001	77260	18970.2
7	2.006	2.032	2.018	76950	18762.6
8	2.035	2.039	2.013	67440	16436.1
9	2.023	2.040	1.987	85400	21068.3
				Average:	17200.8

Table C.15: Compression Results - Sieve 2

Specimen	Average length	Average base	Average height	Max Load (lbs)	Compressive Strength (psi)
1	2.025	2.047	2.002	80000	19518.1
2	2.034	2.043	2.020	68220	16525.3
3	2.017	2.037	1.999	70730	17372.8
4	2.014	2.043	2.008	52700	12842.1
5	2.023	2.041	2.021	60480	14664.7
6	2.037	2.053	2.000	77290	18817.5
7	2.012	2.025	2.009	84670	20809.1
8	2.030	2.025	2.025	79970	19498.7
9	2.013	2.028	2.007	58010	14254.8
				Average:	17144.8

Appendix D: Charpy Results

Table D.1: Charpy Results – Control

Specimen	Average length	Average base	Average height	Max Load (ft-lb)	Energy Absorbed (ft-lb/in)
1	2.026	1.030	1.068	29	27.2
2	2.017	1.034	1.066	18	16.9
3	2.042	1.021	1.071	19	17.7
4	2.026	1.029	1.096	34	31.0
5	2.035	1.024	1.065	40	37.6
6	2.022	1.026	1.073	20	18.6
7	2.048	1.025	1.095	19	17.4
8	2.020	1.018	1.054	26	24.7
9	2.021	1.035	1.091	20	18.3
				Average:	23.3

Table D.2: Charpy Results - Silica Fume 1

Specimen	Average length	Average base	Average height	Max Load (ft-lb)	Energy Absorbed (ft-lb/in)
1	2.017	1.014	1.032	-	0.0
2	2.024	1.026	1.073	55	25.2
3	2.019	1.023	1.008	46	17.9
4	2.010	1.007	1.030	62	33.0
5	2.016	1.009	1.057	60	30.3
6	2.012	1.017	1.044	39	10.5
7	2.017	1.009	1.048	50	21.0
8	2.016	1.020	1.036	40	11.6
9	2.011	1.027	1.062	58	28.2
10	2.017	1.026	1.037	40	11.6
11	2.017	1.023	1.057	44	15.1
12	2.026	1.014	1.031	44	15.5
				Average:	20.0

Table D.3: Charpy Results - Silica Fume 2

Specimen	Average length	Average base	Average height	Max Load (ft-lb)	Energy Absorbed (ft-lb/in)
1	2.030	1.030	1.063	48	18.8
2	2.008	1.035	1.059	56	26.4
3	2.023	1.020	1.070	40	11.2
4	2.021	1.020	1.077	42	13.0
5	2.017	1.016	1.086	47	17.5
6	2.007	1.016	1.084	60	29.5
7	2.005	1.010	1.072	51	21.4
8	2.015	1.023	1.065	74	43.2
9	2.026	1.005	1.049	56	26.7
10	2.018	1.030	1.050	36	7.6
11	2.014	0.999	1.053	37	8.5
12	2.006	1.007	1.060	40	11.3
				Average:	19.6

Table D.4: Charpy Results - Silica Fume 3

Specimen	Average length	Average base	Average height	Max Load (ft-lb)	Energy Absorbed (ft-lb/in)
1	2.005	1.020	1.049	58	28.6
2	2.011	1.021	1.055	40	11.4
3	1.999	1.019	1.065	41	12.2
4	2.009	0.995	1.059	57	27.4
5	2.008	1.022	1.046	54	24.8
6	2.000	1.027	1.049	44	15.2
7	1.985	1.012	1.081	46	16.6
8	2.009	1.005	1.070	62	31.8
9	2.005	1.021	1.059	38	9.4
10	2.020	1.019	1.058	46	17.0
11	2.011	0.994	1.061	52	22.6
12	2.007	1.022	1.048	47	18.1
				Average:	19.6

Table D.5: Charpy Results - Silica Fume 4

Specimen	Average length	Average base	Average height	Max Load (ft-lb)	Energy Absorbed (ft-lb/in)
1	2.001	1.015	1.078	42	13.0
2	2.011	1.010	1.065	44	15.0
3	2.018	1.007	1.077	41	12.1
4	1.998	0.986	1.071	90	57.9
5	2.014	1.022	1.068	48	18.7
6	2.002	1.017	1.078	36	7.4
7	2.006	0.994	1.056	48	18.9
8	2.004	1.021	1.055	47	18.0
9	1.996	1.010	1.089	66	34.9
10	2.009	0.992	1.062	54	24.5
11	2.000	1.015	1.086	44	14.7
12	2.005	1.009	1.101	53	22.7
				Average:	21.5

Table D.6: Charpy Results - Water 1

Specimen	Average length	Average base	Average height	Max Load (ft-lb)	Energy Absorbed (ft-lb/in)
1	2.004	1.015	1.100	48	18.2
2	2.018	1.018	1.083	62	31.4
3	2.016	1.019	1.092	70	38.5
4	2.006	1.014	1.076	72	40.9
5	2.018	1.023	1.072	34	5.6
6	2.018	1.024	1.066	50	20.6
7	2.009	1.016	1.067	43	14.1
8	2.025	1.013	1.077	33	4.6
9	2.016	1.014	1.070	40	11.2
10	2.016	1.016	1.066	55	25.3
11	2.017	1.011	1.071	64	33.6
12	2.013	1.014	1.059	54	24.6
				Average:	22.4

Table D.7: Charpy Results - Water 2

Specimen	Average length	Average base	Average height	Max Load (ft-lb)	Energy Absorbed (ft-lb/in)
1	2.013	1.015	1.067	58	28.1
2	2.015	1.019	1.073	63	32.6
3	2.006	1.022	1.073	51	21.4
4	2.017	1.016	1.053	54	24.7
5	2.014	1.023	1.062	36	7.5
6	2.005	1.017	1.071	59	28.9
7	2.022	1.011	1.046	38	9.6
8	2.010	1.017	1.058	79	48.2
9	2.005	1.010	1.059	74	43.4
10	2.023	1.005	1.040	82	51.9
11	2.010	1.000	1.046	41	12.4
12	2.003	1.000	1.045	36	7.7
				Average:	26.4

Table D.8: Charpy Results - Water 3

Specimen	Average length	Average base	Average height	Max Load (ft-lb)	Energy Absorbed (ft-lb/in)
1	2.009	1.023	1.079	60	29.6
2	2.006	1.030	1.049	40	11.4
3	1.996	1.025	1.062	35	6.6
4	1.993	1.014	1.045	36	7.7
5	1.988	1.014	1.035	39	10.6
6	1.999	1.012	1.045	53	23.9
7	2.012	1.016	1.040	45	16.4
8	1.997	1.008	1.047	50	21.0
9	2.002	1.013	1.050	108	76.2
10	2.010	1.012	1.040	47	18.3
11	2.025	1.012	1.051	71	40.9
12	1.995	1.017	1.040	50	21.1
				Average:	23.6

Table D.9: Charpy Results - Sieve 1

Specimen	Average length	Average base	Average height	Max Load (ft-lb)	Energy Absorbed (ft-lb/in)
1	2.017	1.021	1.088	48	18.4
2	2.022	1.023	1.083	58	27.7
3	2.008	1.025	1.106	57	26.2
4	2.016	1.015	1.065	58	28.2
5	2.018	1.027	1.068	42	13.1
6	2.009	1.030	1.082	52	22.2
7	2.016	1.016	1.063	51	21.6
8	2.016	1.019	1.061	57	27.3
9	2.008	1.013	1.066	100	67.5
10	2.014	1.004	1.054	62	32.2
11	2.004	1.003	1.066	50	20.6
12	2.005	1.000	1.066	56	26.3
				Average:	27.6

Table D.10: Charpy Results - Sieve 2

Specimen	Average length	Average base	Average height	Max Load (ft-lb)	Energy Absorbed (ft-lb/in)
1	2.004	1.015	1.051	72	41.9
2	2.010	1.020	1.056	64	34.1
3	2.019	1.020	1.058	36	7.6
4	2.009	1.014	1.058	34	5.7
5	2.022	1.015	1.069	64	33.7
6	2.019	1.008	1.064	43	14.1
7	2.008	1.011	1.074	43	14.0
8	2.030	1.015	1.085	56	25.8
9	2.015	1.016	1.078	63	32.5
10	2.037	1.019	1.089	42	12.9
11	2.001	1.020	1.060	56	26.4
12	2.011	1.017	1.084	44	14.8
				Average:	21.9